Electronic Supplementary Information

Origin of the polychromatic photoluminescence of zeolite confined Ag clusters: temperature- and co-cation- dependent luminescence

Li Sun,[a] Masoumeh Keshavarz,[a] Giacomo Romolini,[a] Bjorn Dieu,[a] Johan Hofkens,[ac] Flip de Jong,[a] Eduard Fron,[ac]* Maarten B. J. Roeffaers,[b]* Mark Van der Auweraer [ac]*

[a] Chem&Tech – Molecular Imaging and Photonics, KU Leuven, Celestijnenlaan 200F, 3001 Leuven, Belgium
[b] Chem&Tech – Centre for Membrane Separations, Adsorption, Catalysis and Spectroscopy for Sustainable Solutions, KU Leuven, Celestijnenlaan 200F, 3001 Leuven, Belgium
[c] KU Leuven Core Facility for Advanced Spectroscopy, Celestijnenlaan 200F, 3001 Leuven, Belgium

*corresponding authors:
eduard.fron@kuleuven.be,
maarten.roeffaers@kuleuven.be,
mark.vanderauweraer@kuleuven.be

Content:

1. Materials and synthesis

In this study, commercial Na-LTA zeolites (UOP) were used as parent materials possessing a normalized and dehydrated unit cell (N.U.C.) with composition $Na_{12}Si_{12}Al_{12}O_{48}$. A series of mixed Li, Na and Ag cation-exchanged LTA were prepared according to the exchange procedure described in detail as reported.[1] Briefly, 3 g of LTA zeolite powder was suspended in 250 mL of an aqueous lithium nitrate solution (5.8 M, $LiNO_3$ Sigma-Aldrich, ≥99.99%), then the suspension was agitated in an end-over-end shaker at 60 °C over one week. During this procedure, the exchange solution was replaced 3 times with a fresh $LiNO_3$ solution to complete full Li exchange. The Li-LTA sample was collected by filtration using a Büchner filter and washed several times with Milli-Q water. Afterward, a batch of zeolites with different Li and Na content was obtained via partly re-exchanging 250 mg of Li-LTA zeolite with Na^+ overnight, using 100 mL of a sodium nitrate solution (1.65 to 19.84 mM, $NaNO_3$ Sigma-Aldrich, ≥99.99%). The theoretical chemical formula of the dehydrated zeolites is $Li_xNa_{12-x}Si_{12}Al_{12}O_{48}$ (Li_xNa_{12-x}-LTA, x=0, 1, …, 12). Subsequently, one Na^+ in 200 mg of these Li_xNa_{12-x}LTA zeolites were exchanged by one Ag^+ using 100 mL of a silver nitrate solution (1.17 to 1.32 mM, $AgNO_3$ Sigma-Aldrich, ≥99.99%). Hence Ag_1-exchanged Li_xNa_{12-x}-LTA zeolite samples denoted as $Ag_1Li_xNa_{11-x}$-LTA (x=0, 1, …, 11) were obtained. Finally, the Ag exchanged zeolites were activated overnight to form Ag clusters (AgCLs) in a muffle oven at 450 °C, starting from room temperature with a heating rate of 5 degrees per minute. In order to avoid zeolite framework destruction by too fast water removal, two 30 min intervals at 80 °C and 110 °C were set.[2] After heat-treatment, these samples were cooled to room temperature in an ambient atmosphere for hydration and then stored in the dark for further analysis.

To obtain dehydrated $Ag_1Li_6Na_5$-LTA, after the same calcination at 450 °C overnight, the sample was quickly transferred to a vial and kept heated at 450 °C for another 60 minutes. Afterwards, the vial was taken out of the oven and immediately sealed with a silica stopper. Upon cooling down, the sample was transferred to a quartz tube inside a glovebox and carefully sealed for the spectroscopic experiments.

Hydrated $Ag_1Li_6K_5$-LTA sample can be prepared by using potassium nitrate (KNO_3) in a similar ion-exchange and heat-treatment procedure.

2. Characterization

2.1 Emission/excitation spectra and photoluminescence quantum yield (PLQY)

The steady-state luminescence properties, including two-dimensional (2D) excitation-emission plots and room-temperature (RT, 298 K) photoluminescence quantum yields (PLQYs), were recorded on an Edinburgh FLS980 fluorimeter with samples placed in a quartz tube (5 mm diameter) and a quartz cuvette (1 mm path length) respectively. 2D emission-excitation plots were also observed at liquid nitrogen temperature (LNT, 77 K). For an excitation wavelength of 265 nm more detailed temperature-dependent photoluminescence measurements (T-dependent PL) were also performed on this setup by connecting an external cryostat (Linkam Scientific Instrument system: T96-S) to the fluorimeter. Samples encapsulated between two quartz plates were placed inside the chamber of the temperature stage (HFS600) which was connected to a Dewar filled with liquid nitrogen and a temperature controller (LNPS96-S). At RT, the PLQY was measured at the maximum of the excitation spectra using an integrating sphere (Labsphere, 100 mm diameter) coupled to the aforementioned fluorimeter through optical fibers. At LNT, the PLQY was measured by coupling the integrating sphere to a Horiba Jobin Yvon Fluorolog fluorimeter. Barium sulfate was adopted as a fully scattering reference for the PLQY measurement.

2.2 Diffuse reflection spectra (DRS)

The diffuse reflectance spectra (DRS) at RT/LNT were performed on a Horiba Jobin Yvon Fluorolog fluorimeter. Quartz tubes containing the samples were placed in a Dewar flask without/with liquid nitrogen. Barium sulfate and black carbon powders were used as 100% and 0% reflective references, respectively. The reflectance percentage of the DRS was finally transformed into Kubelka-Munk (K-M).

2.3 Thermogravimetric analysis

Thermogravimetric analysis (TGA) was implemented on a TA Instruments Q500 thermogravimetric analyzer to monitor the water loss behavior of hydrated samples after dehydration. The zeolite samples (15-25 mg) were heated under nitrogen gas flow (90 mL/min) until 700 °C with a liner heating ramp of 10°C/min. TA Universal Analysis software was used for analysis.

2.4 Elemental analysis

The elemental analysis of different zeolite samples was conducted by inductively coupled plasma-optical emission spectrometry (ICP-OES) and atomic absorption spectroscopy (AAS), aiming to figure out Ag content and Li/Na composition respectively. ICP-OES was performed using a Varian 720-ES instrument and AAS using a Varian SpectrAA 20 plus. After analysis of the weight percentage (wt%), the element content was determined by normalizing the combined charge of all cations (Ag=1, Li+Na=11) to 12.

2.5 X-ray diffraction measurement

X-ray diffraction (XRD) measurements were performed on a Malvern PANalytical Empyrean diffractometer using Cu Kα1 radiation (λ=1.5406 Å).

2.6 Time-resolved spectroscopy

2.6.1 Time-correlated single-photon counting (TCSPC)

Time-correlated single-photon counting (TCSPC) was used to determine the luminescence decays at the pico-nanosecond time scale. Samples were enclosed in sealed quartz tubes for the experiments at 298 K and 77 K. The frequency-tripled output (266 nm, 8.18 MHz, 2 ps FWHM) of a mode-locked Ti: Sapphire laser (Tsunami, Spectra Physics) was chosen as the excitation source. The linearly polarized excitation light was rotated to a vertical direction by using a Berek compensator (New Focus) in combination with a polarizer and directed onto the sample. The emission was collected under 90° with respect to direction of the incident light and guided through a polarizer that was set at the magic angle (54.7°) with respect to the polarization of the excitation

beam. The fluorescence was spectrally resolved by a monochromator (Sciencetech 9030, 100 mm focal length, wavelength accuracy 0.3 nm), and detected by a microchannel plate photomultiplier tube (MCP-PMT, R3809U-51, Hamamatsu). A time-correlated single photon timing PC module (SPC 830, Becker & Hickl) was used to obtain the fluorescence decay histogram in 4096 channels. The decays were recorded with 10000 counts in the peak channel, in a time window of 26 ns corresponding to 6.34 ps per channel. A time-resolved fluorescence analysis (TRFA) software based on iterative reconvolution of the data with the instrumental response function (IRF) was applied to analyze these decays. The full width at half- maximum (FWHM) of the IRF was typically in the order of 42 ps. The quality of the fits was judged by the fit parameters χ^2 (<1.2), Z^2 (<3) and the Durbin Watson parameter (1.8<DW<2.2) as well as by the visual inspection of the residuals and their autocorrelation function.

2.6.2 Nanosecond to millisecond time-resolved luminescence

Zeolite samples were encapsulated between two quartz plates and filled in quartz tubes for measurement of temperature-dependent time-resolved luminescence by using the Linkam Scientific Instrument system (T96-S) as mentioned before for temperature control. They were excited using laser pulses generated by a Nd: YAG laser (Quanta-Ray INDI-40, Spectra Physics, 355 nm) pumping an optical parametric oscillator (OPO，basisScan/120, GWU-Lasertechnik). The excitation light was set to 265 nm by doubling the output of the OPO (530 nm) using a home-made doubler and wavelength separator to suppress the residual light. The obtained excitation light was focused on the sample using a lens (focal length ~300 mm). A fraction of the excitation light was sent to a fast photodiode for generating an electronic trigger. The emitted luminescence was collected at a right-angle configuration, filtered with a long-pass filter (360 nm) and focused on the entrance slit of a spectrograph with a focal length of 300 mm (SpectroPro-300i, Acton Research). A photomultiplier tube (PMT) (Hamamatsu, R928) mounted at one exit port of the spectrograph was used as detector. The width of the entrance and exit slits of the spectrograph were set to 0.5 mm. The electrical signal was sent to an oscilloscope with a 50-Ohm entrance to obtain the transient electrical

signal. The time resolution of the experiment was estimated to 10 ns using scattered light. A homemade software based on LabView was used to control and trigger the instruments, and to read, average and store the data. The time windows used here were 200 μs and 2 ms.

3. Supplementary Figures, Tables and relevant text

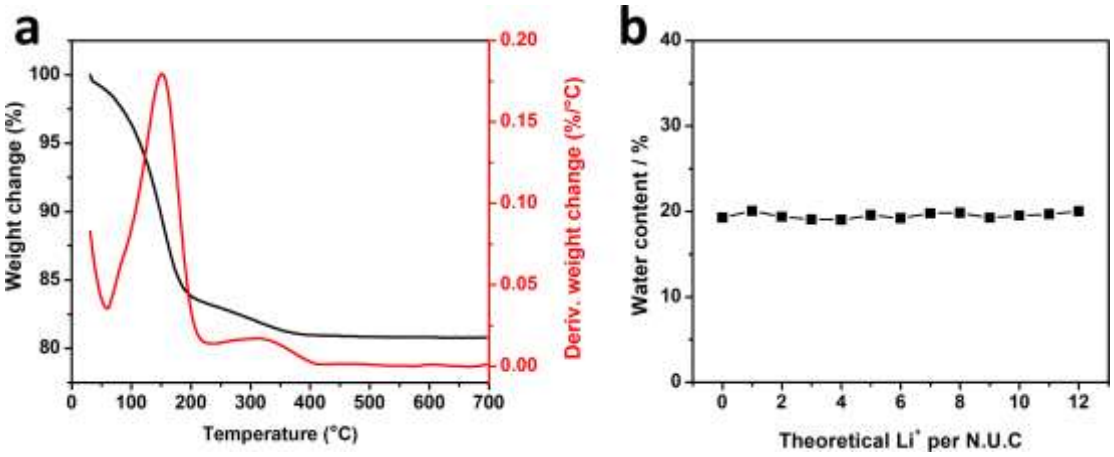

Figure S1. (a) Thermogravimetric analysis (TGA) of a hydrated $Ag_1Li_6Na_5$-LTA sample and (b) the water content of all Ag_1-exchanged Li_xNa_{12-x}-LTA (x=0-12) zeolites. The latter plot shows that they all have a similar hydration level with a water content around 20 wt%.

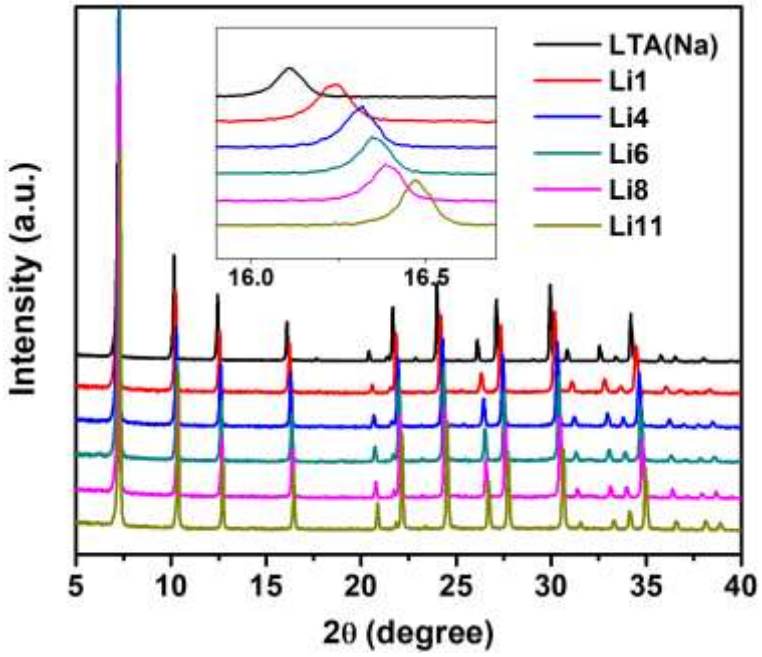

Figure S2. X-ray diffraction (XRD) of neat LTA (Na) and Ag_1-exchanged Li_xNa_{12-x}-LTA (x=1, 4, 6, 8, 11) samples at 298 K.

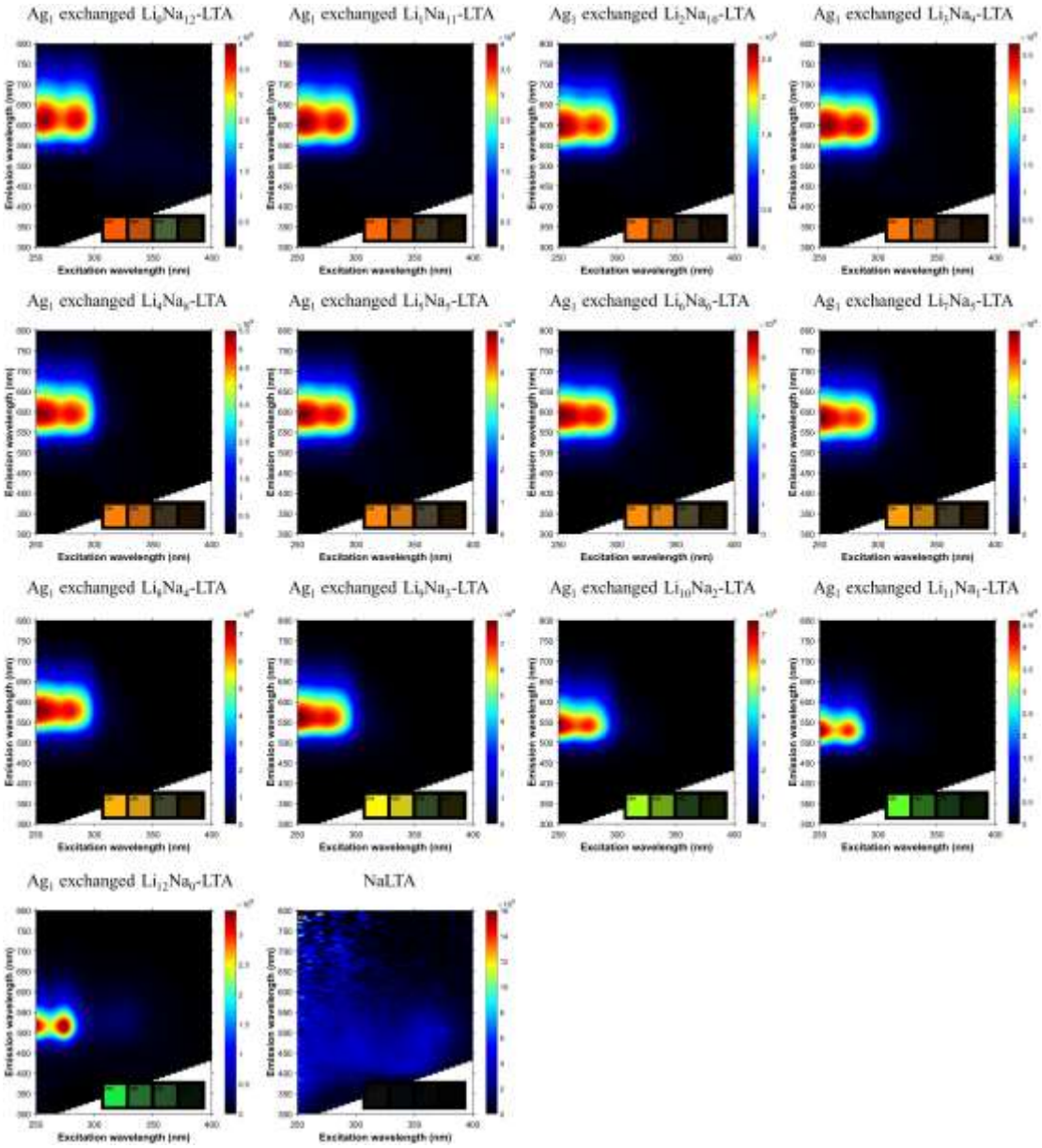

Figure S3. Two-dimensional excitation/emission plots of the hydrated Ag_1-exchanged Li_xNa_{12-x}-LTA (x=0-12) samples and a neat NaLTA zeolite sample at 298 K.

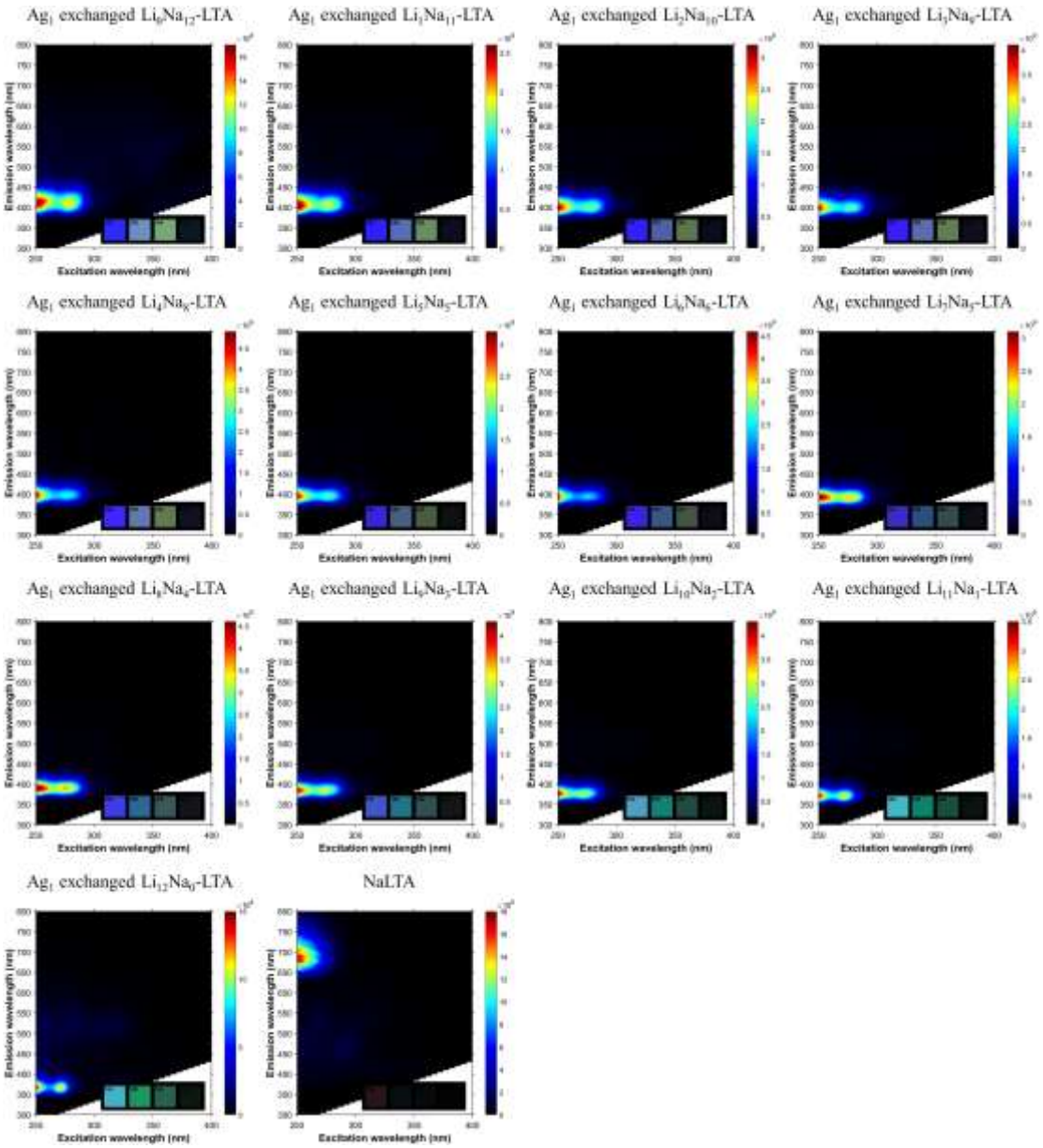

Figure S4. Two-dimensional excitation/emission plots of the hydrated Ag_1-exchanged Li_xNa_{12-x}-LTA (x=0-12) samples and a neat NaLTA zeolite sample at 77 K.

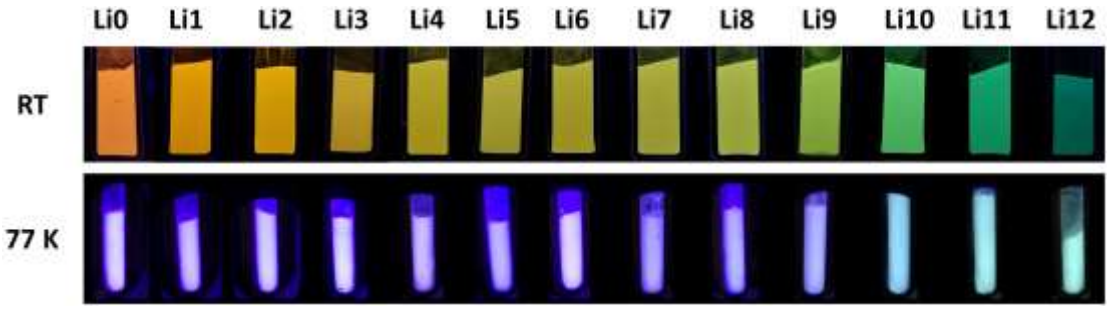

Figure S5. Images of the luminescent Ag_1-exchanged Li_xNa_{12-x}-LTA (x=0-12) zeolites (simply denoted as Li_x: x=0-12) at 298 K (RT) and 77 K under a UV lamp (ex255 nm). The emission color varies from orange to blue upon increasing the Li content at RT, while it doesn't change significantly at 77 K. Note that the violet is missing from Li_{10} to Li_{12} at 77 K, this is because their maximum emissions (<380 nm) are beyond the visible light range.

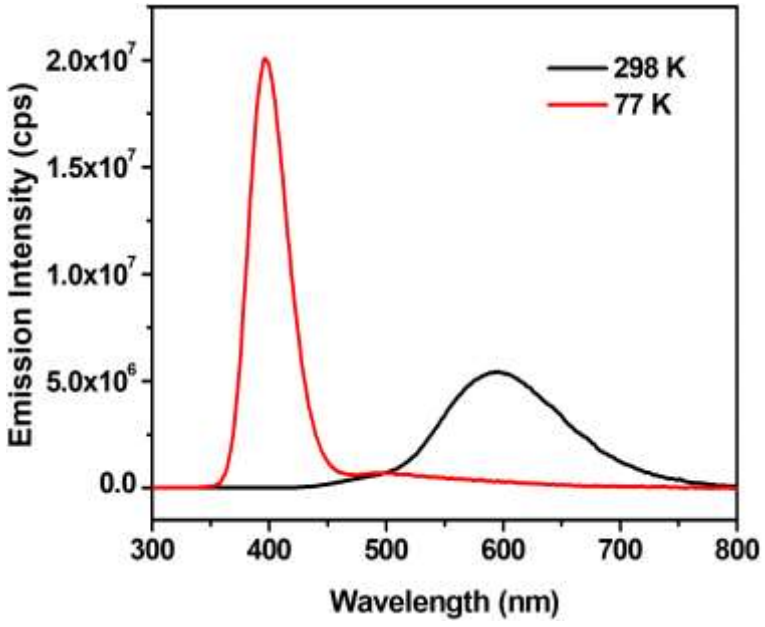

Figure S6. The emission spectra of $Ag_1Li_6Na_5$-LTA at 298 K and 77 K under 265 nm excitation.

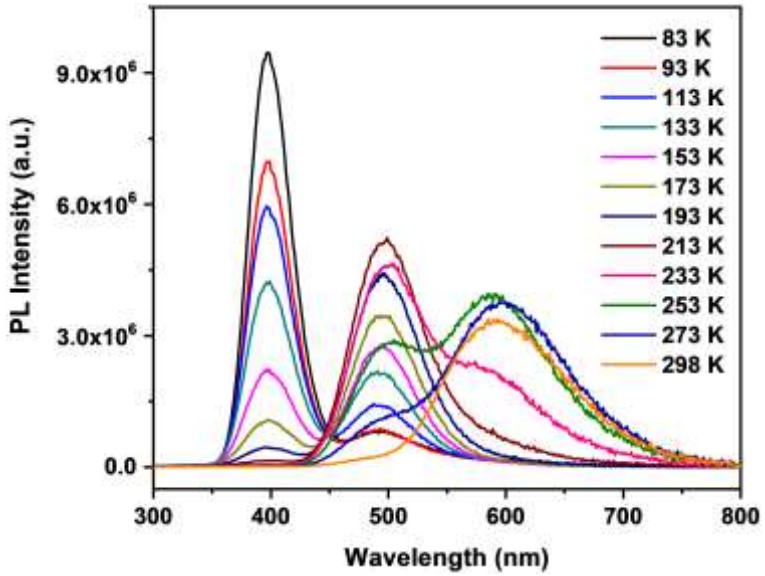

Figure S7. Temperature-dependent photoluminescence spectra of $Ag_1Li_6Na_5$-LTA with temperature increasing from 83 K to 298 K under 265 nm excitation. This change has been shown to be reversible.

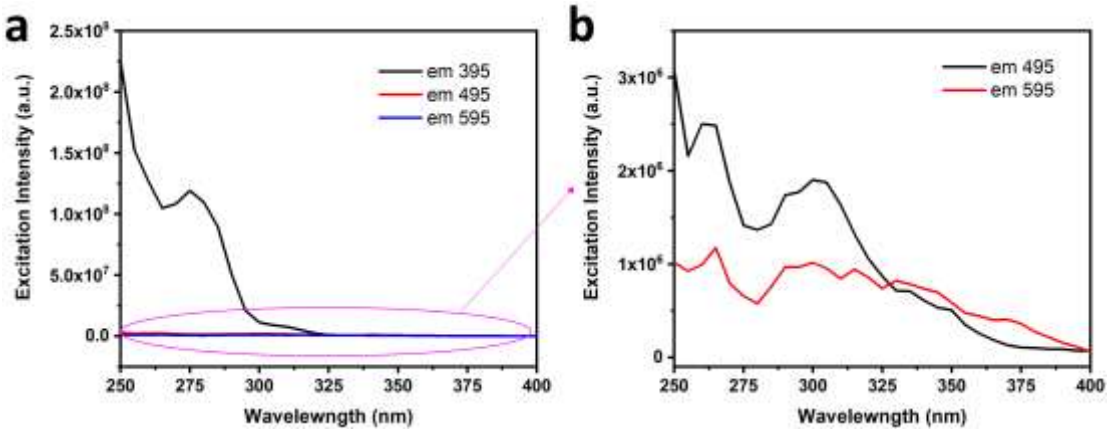

Figure S8. The excitation spectra of $Ag_1Li_6Na_5$-LTA at 77 K (detected at 395 nm, 495 nm and 595 nm).

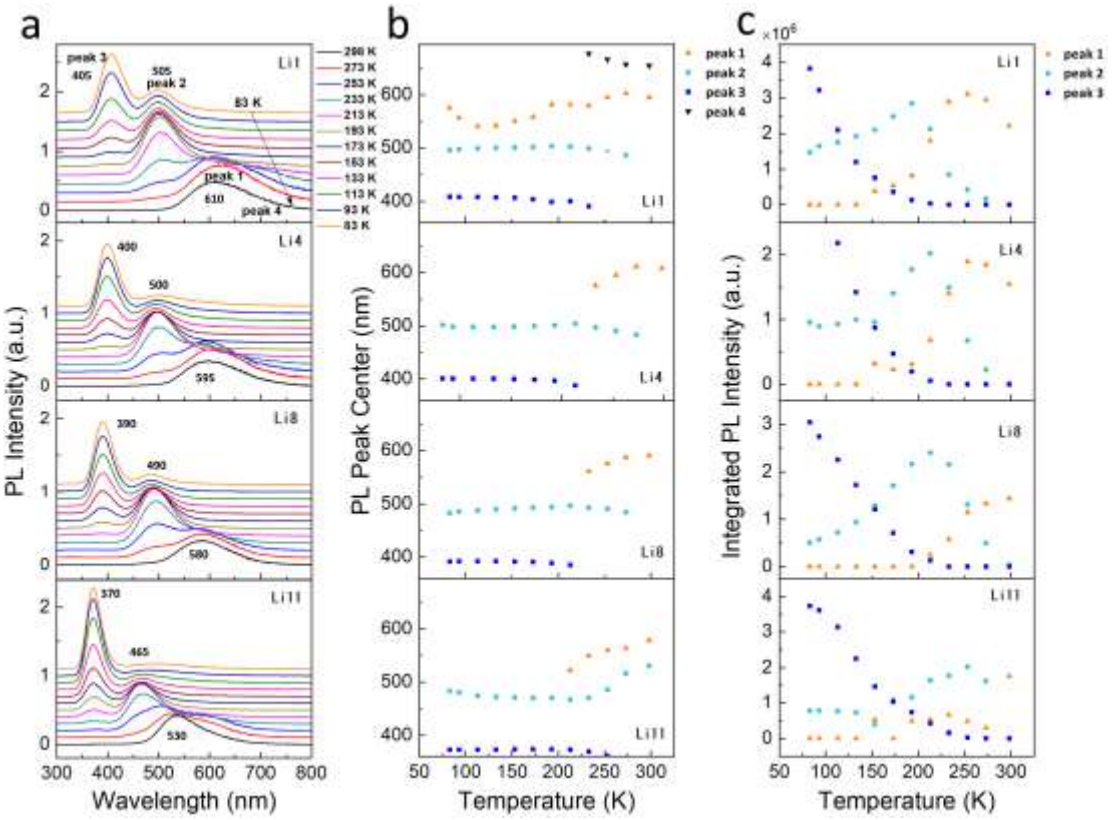

Figure S9. (a) Temperature-dependent photoluminescence spectra of Ag_1-exchanged Li_xNa_{12-x}-LTA (x=1, 4, 8, 11) zeolites for temperature ranging from 298 K to 83 K under 265 nm excitation; the peaks that appear sequentially as the temperature decreases are named peak 1, peak 2, and peak 3 (peak 4 was only observed for $Ag_1Li_1Na_{10}$-LTA: ~700 nm). (b) Peak position and (c) integrated peak intensity at different temperatures. Figure S8c as well as Figure 1f show the integrated PL intensity of the different peaks as a function of temperature. This integrated intensity was determined through Gauss fits to the PL spectra.

Photoluminescence investigation of dehydrated $Ag_1Li_6Na_5$-LTA sample at RT and 77 K

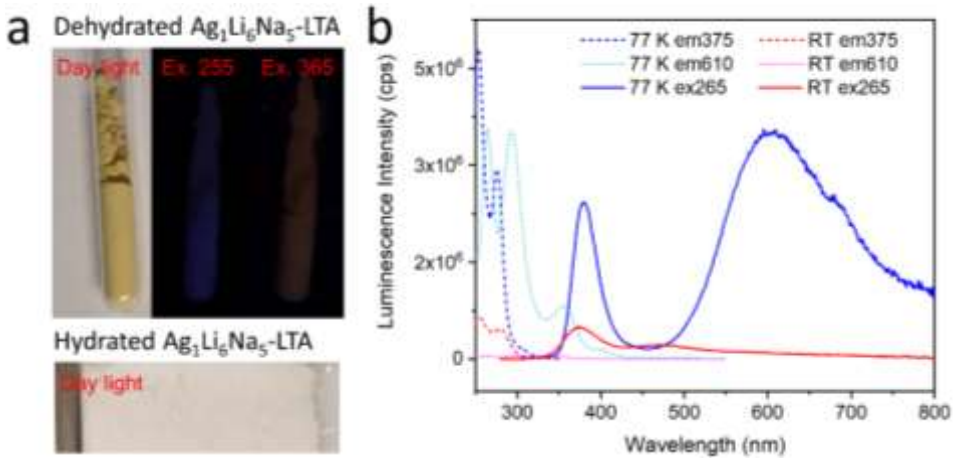

Figure S10. (a) The photographs of (de)hydrated $Ag_1Li_6Na_5$-LTA under daylight and/or a UV-lamp (excitation wavelength: 255 and 365 nm) at RT; (b) The excitation and emission spectra of dehydrated $Ag_1Li_6Na_5$-LTA sample measured at RT and 77 K respectively.

In order to explore the role of water molecules incorporated in the zeolite the spectroscopy of the silver clusters in a hydrated and dehydrated sample of $Ag_1Li_6Na_5$-LTA were compared.

The dehydrated sample was obtained by calcination at 450 °C overnight. The sample was then quickly transferred to a vial and keep heated at 450 °C for another 60 minutes. Afterwards, the vial was taken out of the oven and immediately sealed with a silica stopper. Upon cooling down, the sample was transferred to a quartz tube inside a glovebox and carefully sealed for the spectroscopic experiments.

At RT, the dehydrated $Ag_1Li_6Na_5$-LTA shows a yellow color under daylight (Figure S10) which is different from the hydrated sample which is a white powder. This behavior is analogous to what was earlier reported for Ag_3Na_9LTA.[3] This indicates the strong coordination of AgCLs with O_F (framework oxygens) upon the loss of water, leading to the deactivation of the luminescent AgCLs to AgCLs with weak/no luminescence. In the hydrated state, the water ligands play a role as protecting shell of the clusters blocking the coordination with LTA framework oxygens, resulting in the

intense luminescence as shown in the manuscript. For the dehydrated $Ag_1Li_6Na_5$-LTA we can observe a weak luminescence at RT with a maximum at 375 nm. This weak 375 nm emission has excitation maxima around 255 and 275 nm (the same as the excitation maxima of the hydrated sample). At 77 K, the intensity of the emission with the maximum at 375 nm increased significantly and a second even more intense band with maximum at 610 nm was observed. For both bands the maximum of the excitation spectrum remained between 255 and 275 nm. The 610 nm emission at 77 K could be attributed to the formation of Ag_6 clusters in dehydrated LTA zeolite of which the intensity increased at 77 K.[3] The behavior of the dehydrated sample resembles strongly that of the dehydrated sample of Ag_3Na_9LTA discussed previously.[3]

The role of the counter ions on the photoluminescence

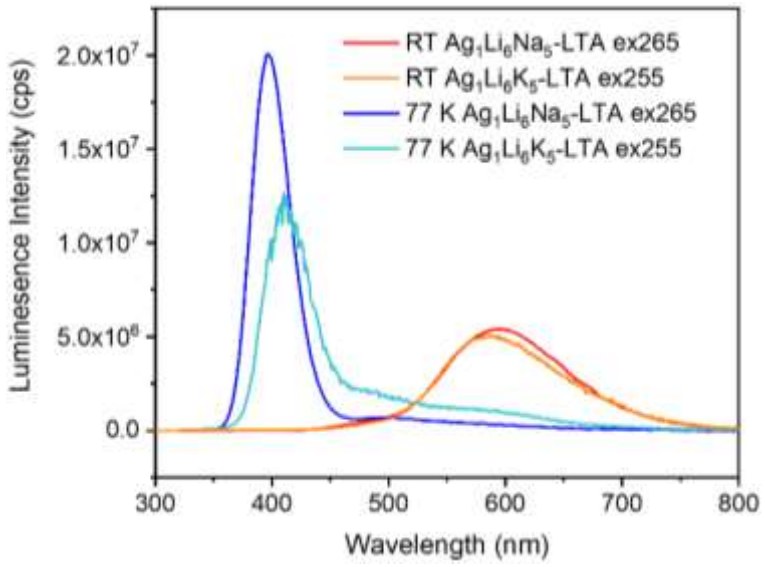

Figure S11. Emission spectra of hydrated $Ag_1Li_6K_5$-LTA (excitation at 255) and hydrated $Ag_1Li_6Na_5$-LTA (excitation at 265 nm) at RT and 77 K.

At RT the emission maximum (excitation 255 nm) is situated at 585 nm which is 10 nm shorter than observed for $Ag_1Li_6Na_5$-LTA. In analogy with $Ag_1Li_6Na_5$-LTA, a blue shift of the maximum to 410 nm is observed upon cooling the sample to 77 K. This is 10 nm longer than observed for $Ag_1Li_6Na_5$-LTA at 77 K (Figure S11). However in contrast to $Ag_1Li_6Na_5$-LTA, the emission spectrum of $Ag_1Li_6K_5$-LTA shows at 77 K also a small shoulder between 450 and 550 nm. In an analogy to our data the presence of two different bands (one around 410 and one around 450-550 nm) at 77 K suggests the presence of several excited state species related to different minima in the potential energy surface of the excited state. The difference between the 77 K spectra of $Ag_1Li_6K_5$-LTA and $Ag_1Li_6Na_5$-LTA also suggests a faster relaxation to T_1, i.e. a smaller energy barrier separating T_3, T_2 and T_1.

The similar behavior of the spectra of $Ag_1Li_6K_5$-LTA and $Ag_1Li_6Na_5$-LTA strongly suggests that also the $Ag_1Li_6K_5$-LTA sample will be characterized by the same temperature-dependent polychromatic photoluminescence as described in our manuscript.

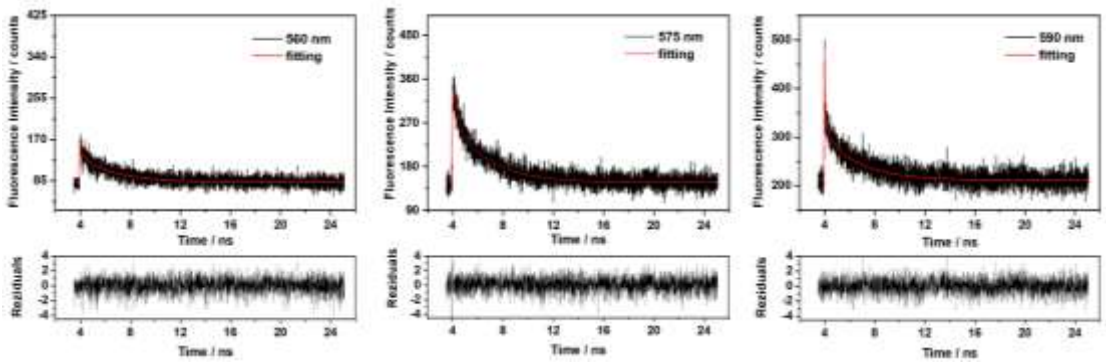

Figure S12. Luminescence decay traces obtained by the time-correlated single-photon counting (TCSPC) and the corresponding fittings as a bi-exponential decay for $Ag_1Li_6Na_5$-LTA, at 298 K in a 26-ns time window (λ_{ex}=318 nm, λ_{det}=545-635 nm). The recovered decay times amount to 0.33 ns and 2.97 ns.

As discussed in the main text, the 2.97 ns component responsible for the major part of the ps-ns emission at 298 K, has a maximum around 580 nm. In spite of the features of its AWD resembling the stationary emission spectrum at 298 K, it is however not straightforward to attribute this component to fluorescence of the singlet excited state 1 (S_1). In this case the internal conversion from S_3 over S_2 to S_1 would occur at 298 K on picosecond time scale, which is four or more orders of magnitude faster than the analogous conversion from T_3 over T_2 to T_1 at 298 K (see main text). An alternative and more likely approach is the attribution of the 2.97 ns component at 580 nm to a small population of clusters differing in nuclearity, geometry or coordination with the LTA lattice and/or water molecules from the AgCL responsible for the stationary emission in this wavelength range.

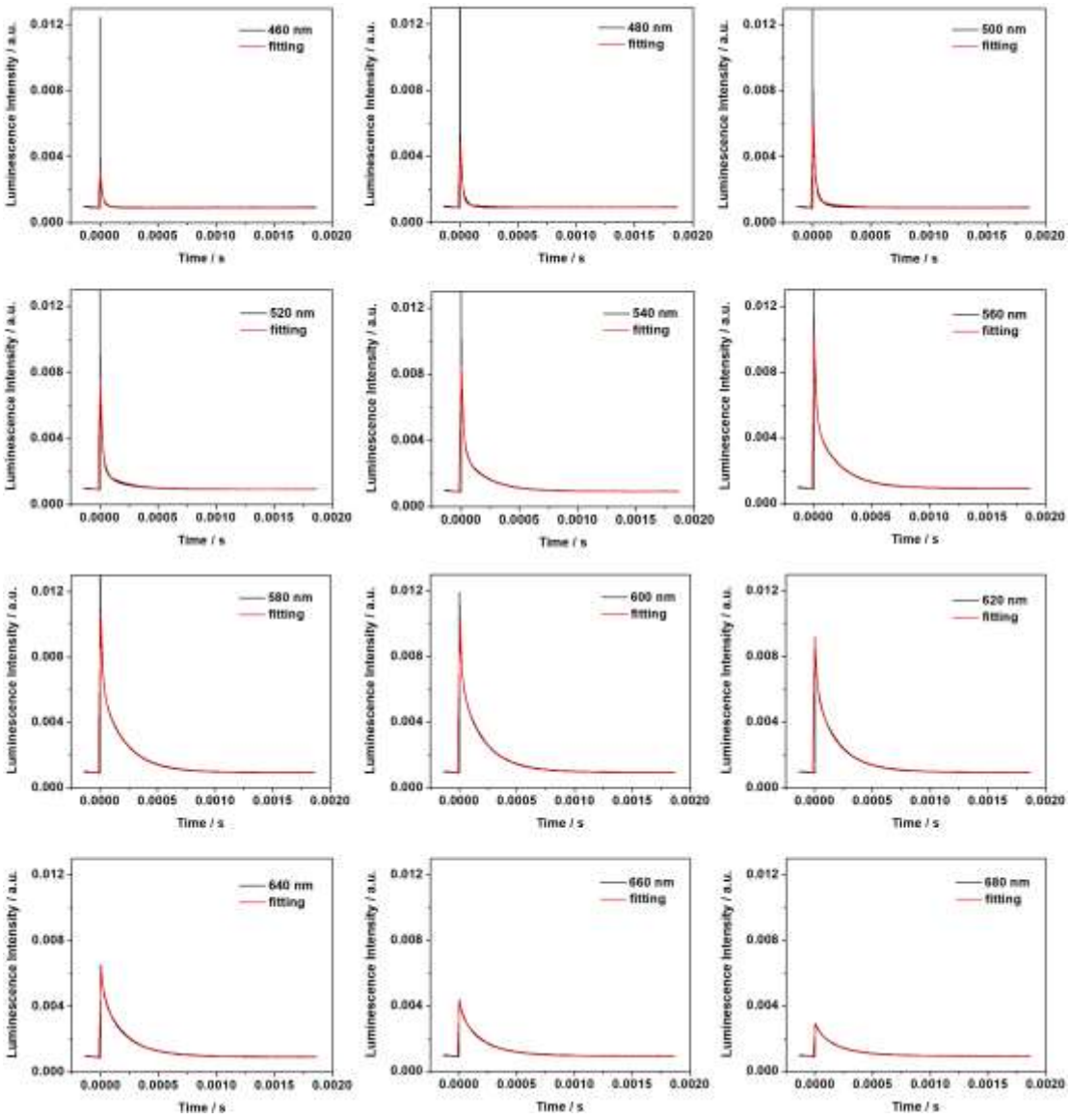

Figure S13. Luminescence decay traces obtained by the ns-ms time-resolved luminescence technique and the corresponding fittings to a multi-exponential decay for $Ag_1Li_6Na_5$-LTA, at 298 K in a 2-ms time window (λ_{ex}=265 nm, λ_{det}=400-760 nm).

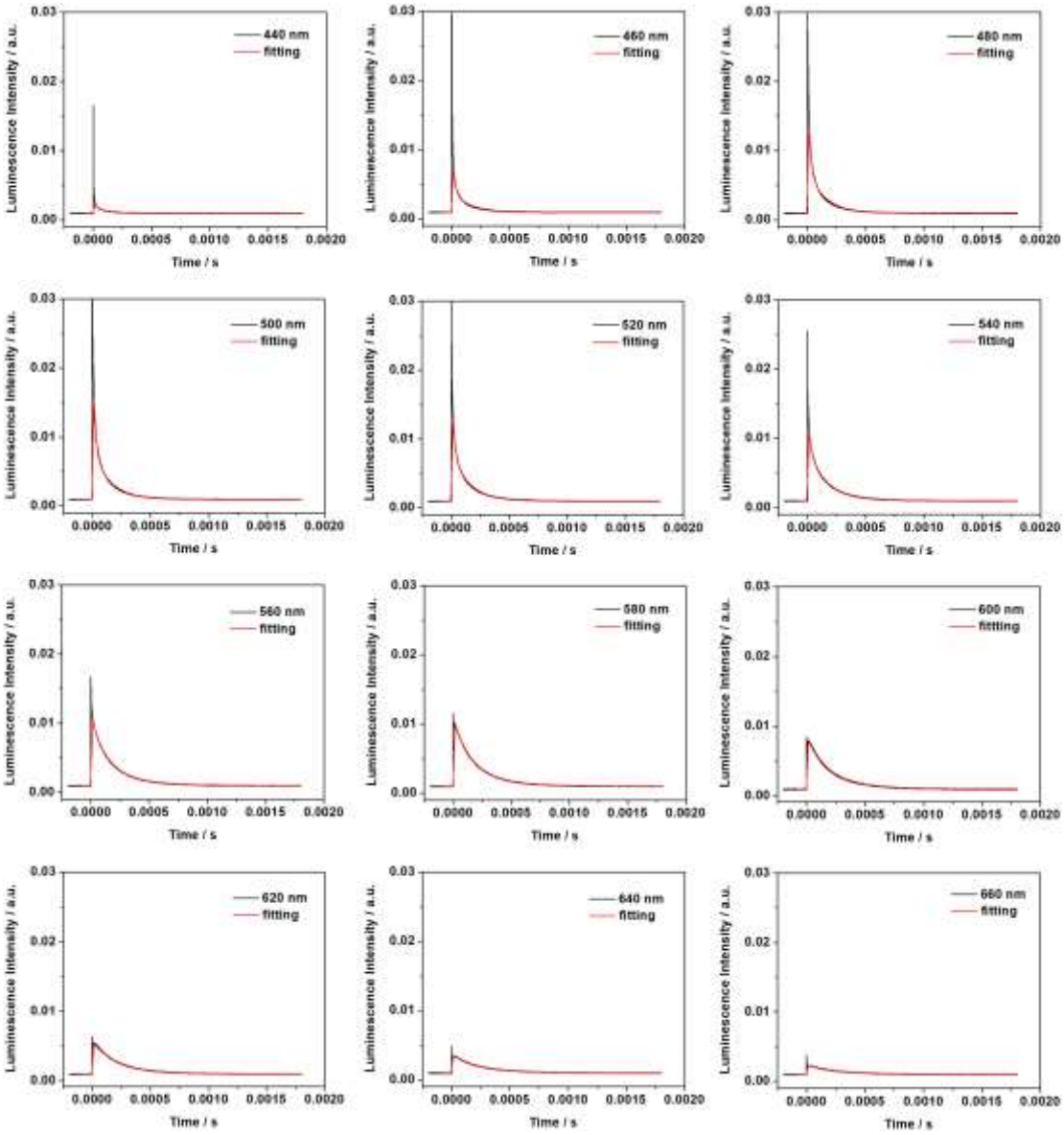

Figure S14. Luminescence decay traces obtained by the ns-ms time-resolved luminescence technique and the corresponding fittings to a multi-exponential decay for $Ag_1Li_6Na_5$-LTA, at 253 K in a 2-ms time window (λ_{ex}=265 nm, λ_{det}=440-720 nm).

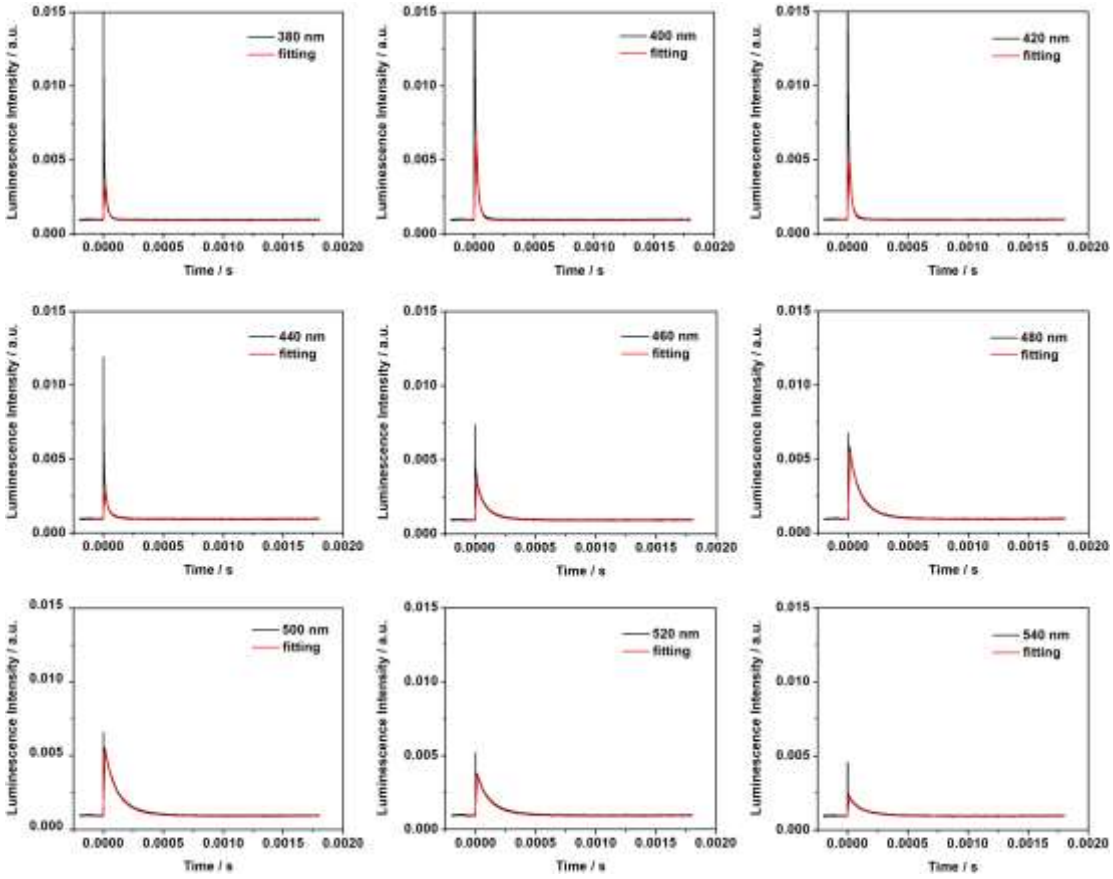

Figure S15. Luminescence decay traces obtained by the ns-ms time-resolved luminescence technique and the corresponding fittings to a multi-exponential decay for $Ag_1Li_6Na_5$-LTA, at 153 K in a 2-ms time window (λ_{ex}=265 nm, λ_{det}=380-580 nm).

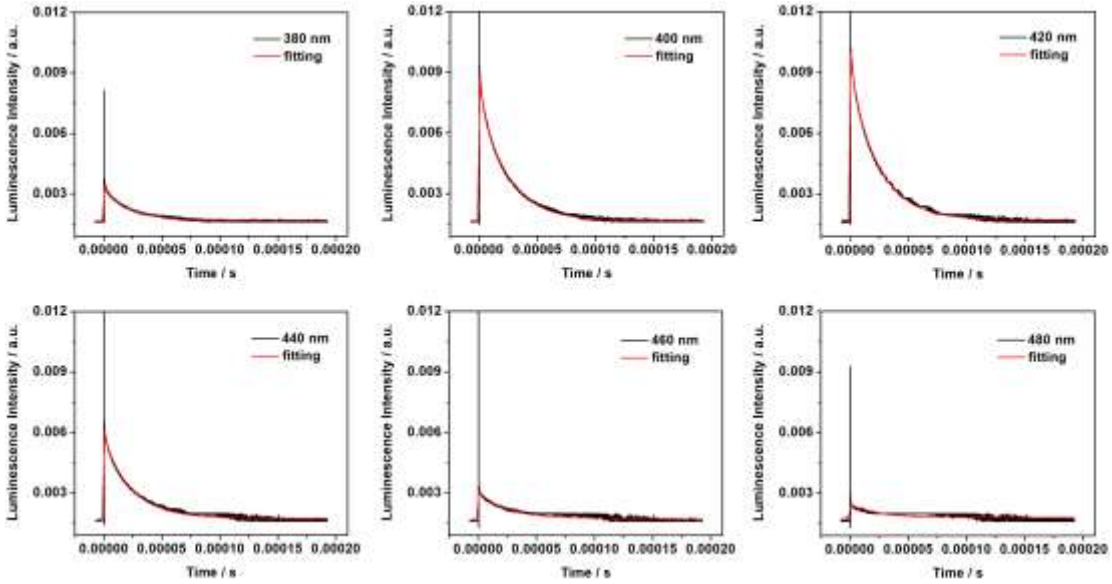

Figure S16. Luminescence decay traces obtained by the ns-ms time-resolved luminescence technique and the corresponding fittings to a multi-exponential decay for $Ag_1Li_6Na_5$-LTA, at 77 K in a 200-μs time window (λ_{ex}=265 nm, λ_{det}=380-480 nm).

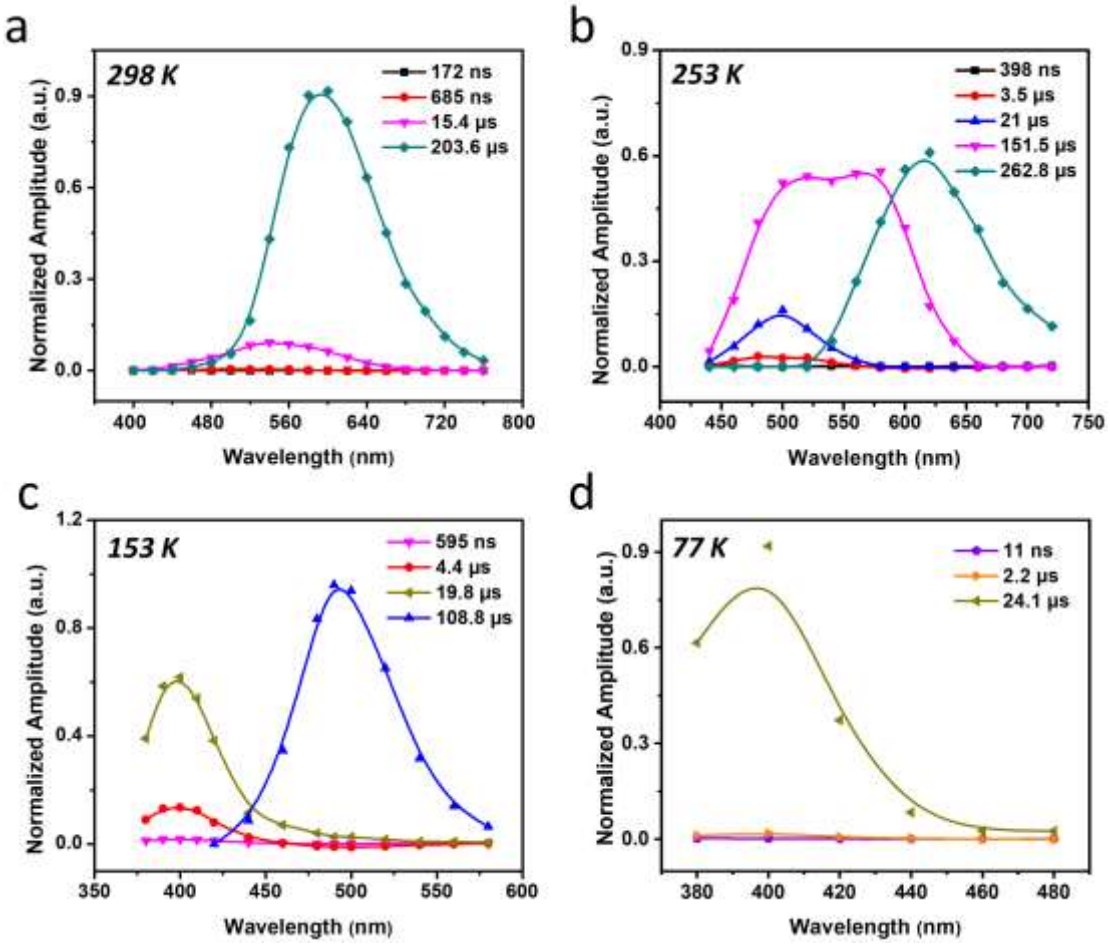

Figure S17. The decay associated spectra (DAS) obtained by the ns-ms time-resolved luminescence technique for $Ag_1Li_6Na_5$-LTA at (a) 298 K, (b) 253 K, (c) 153 K and (d) 77 K in a 2-ms and 200-µs time window (λ_{ex}=265 nm, λ_{det}=380-760 nm).

For the components with a decay time of 172 ns (298 K), 398 ns (253 K) and 595 ns (153 K), one should note that they all contribute much less than 1% to the total emission intensity. As the total PLQY at 77 K amounts to 0.73 and as 95% of this emission is due to the species with a decay time of 24.1 µs at least 69% of the absorbed photons populate this species. If the intrinsic PLQY of this species is less than one even a larger fraction of the absorbed photons are channeled to this species. This means that at best a minor fraction of the absorbed photons is channeled to the species with decay times ranging from 172 ns at 298 K to 595 ns at 153 K which were tentatively attributed to an impurity or to clusters with a slightly different structure and low abundance.

Explanation of the negative amplitude at wavelength longer than 600 nm.

The general function used in the fit analysis is a multi-exponential decay function with the form:

$$I_{(t)} = \sum_{i=1}^{n} A_i \exp(-\frac{t}{\tau_i})$$

where A_i is the amplitude or pre-exponential factor and $\tau(t)$ is the time constant. When a time resolved luminescence signal displays a rising part due to fact that the emitting species is generated by decay of a precursor, the fit analysis detects this rise as a decay component with a negative amplitude. This suggests that the emission attributed to that state is first being formed with a time constant $\tau(i)$ and a corresponding amplitude A_i. In a very simplistic manner, the scheme bellow indicates the luminescence signal expected when T_1 is formed with 685 ns time constant from T_2 while T_1 decays with a time constant 203.5 μs. The time profile observed for T_1 corresponds to that expected for the intermediate in case of two consecutive first order reactions.

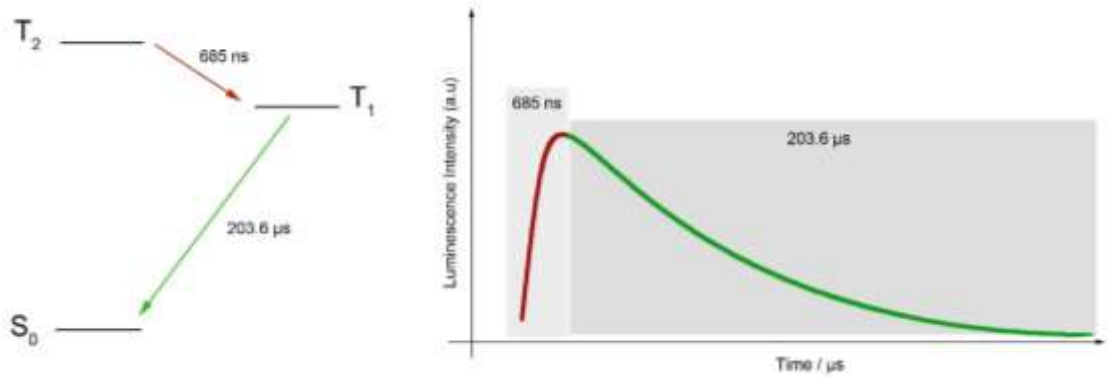

Figure S18. Kinetic scheme and related time-dependent luminescence signal for a process with negative amplitude of the pre-exponential factor.

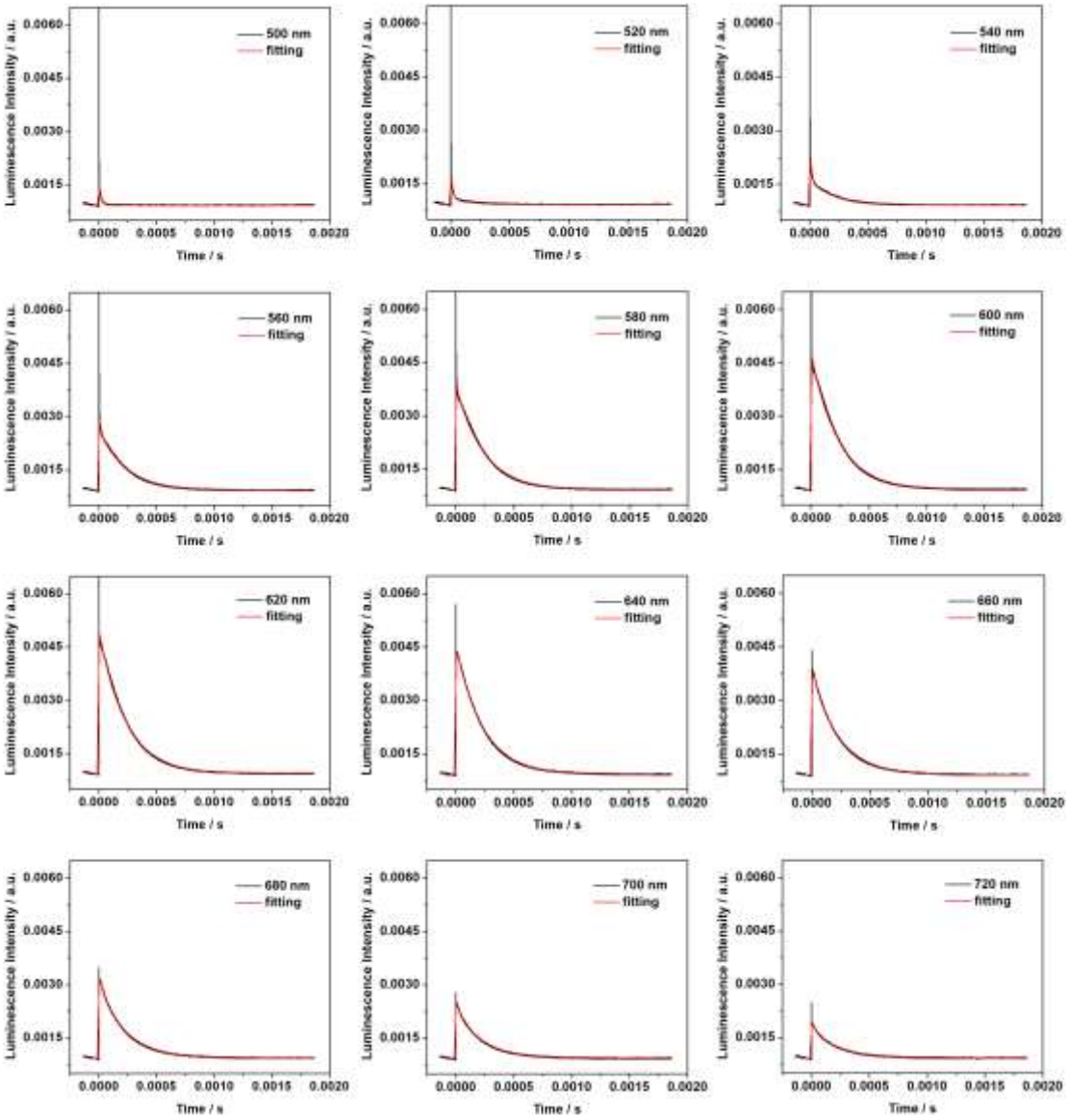

Figure S19. Luminescence decay traces obtained by the ns-ms time-resolved luminescence technique and the corresponding fittings to a multi-exponential decay for $Ag_1Li_0Na_{11}$-LTA, at 298 K in a 2-ms time window (λ_{ex}=265 nm, λ_{det}=500-720 nm).

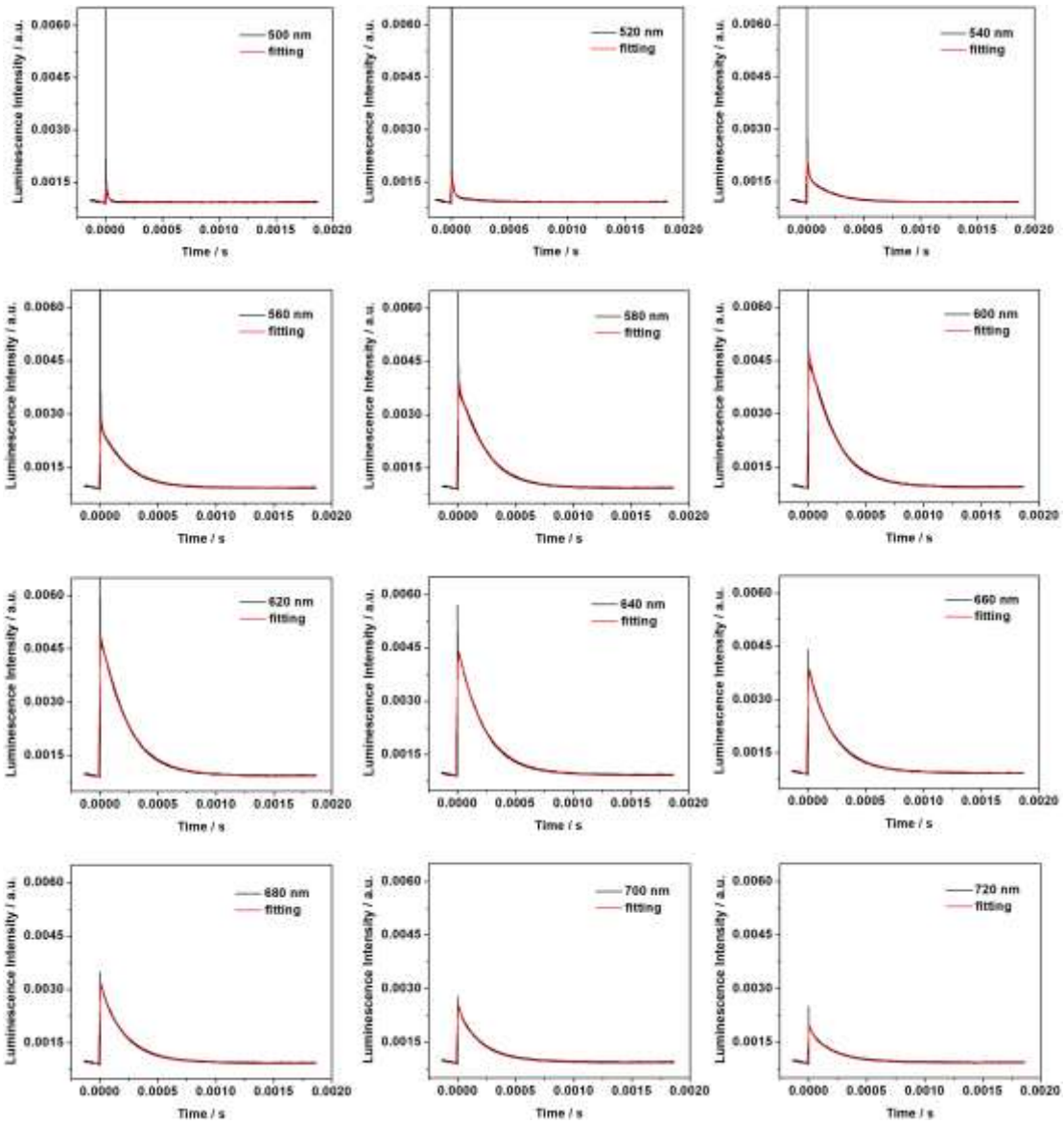

Figure S20. Luminescence decay traces obtained by the ns-ms time-resolved luminescence technique and the corresponding fittings to a multi-exponential decay for $Ag_1Li_1Na_{10}$-LTA, at 298 K in a 2-ms time window (λ_{ex}=265 nm, λ_{det}=500-720 nm).

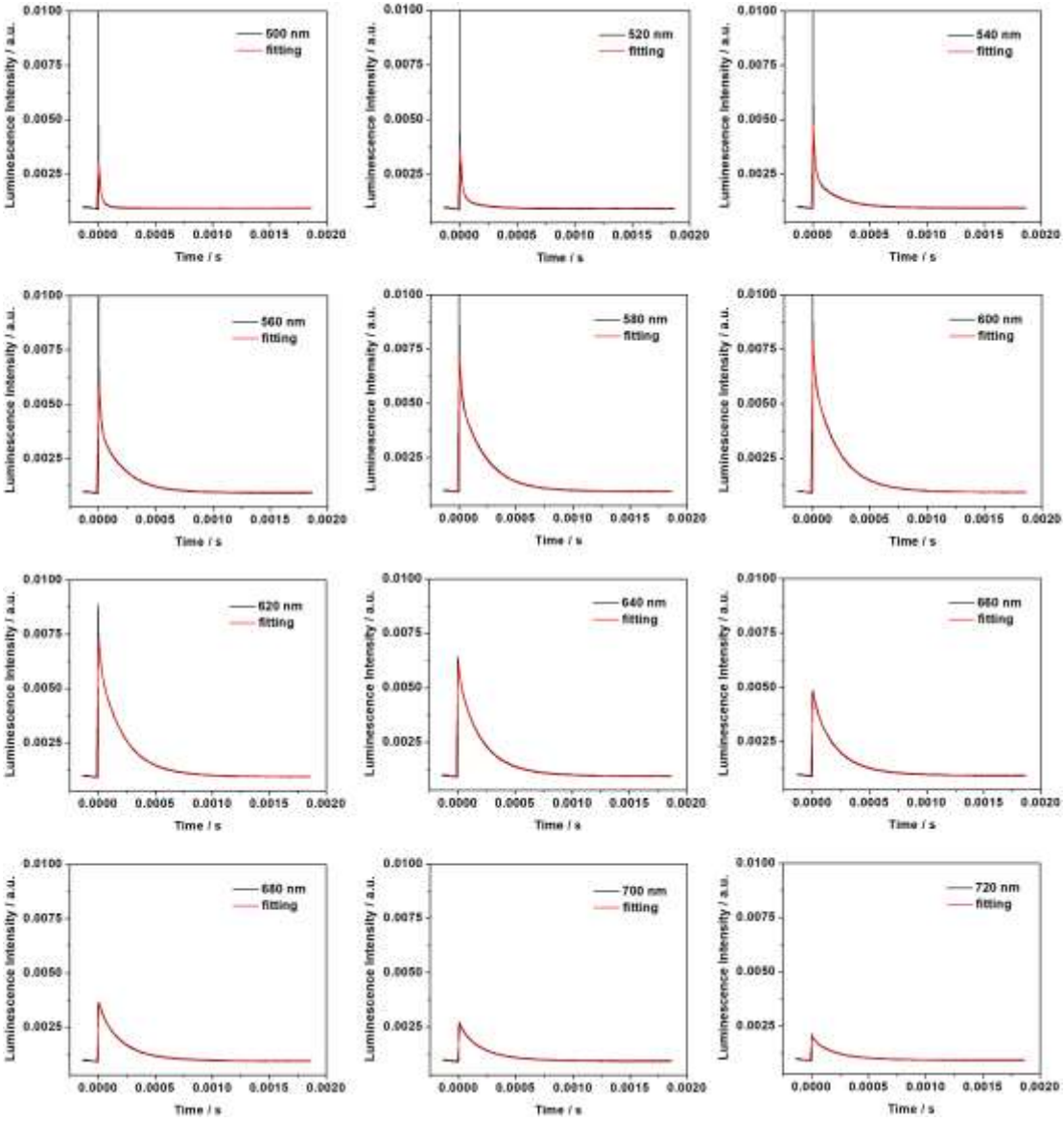

Figure S21. Luminescence decay traces obtained by the ns-ms time-resolved luminescence technique and the corresponding fittings to a multi-exponential decay for $Ag_1Li_2Na_9$-LTA, at 298 K in a 2-ms time window (λ_{ex}=265 nm, λ_{det}=500-720 nm).

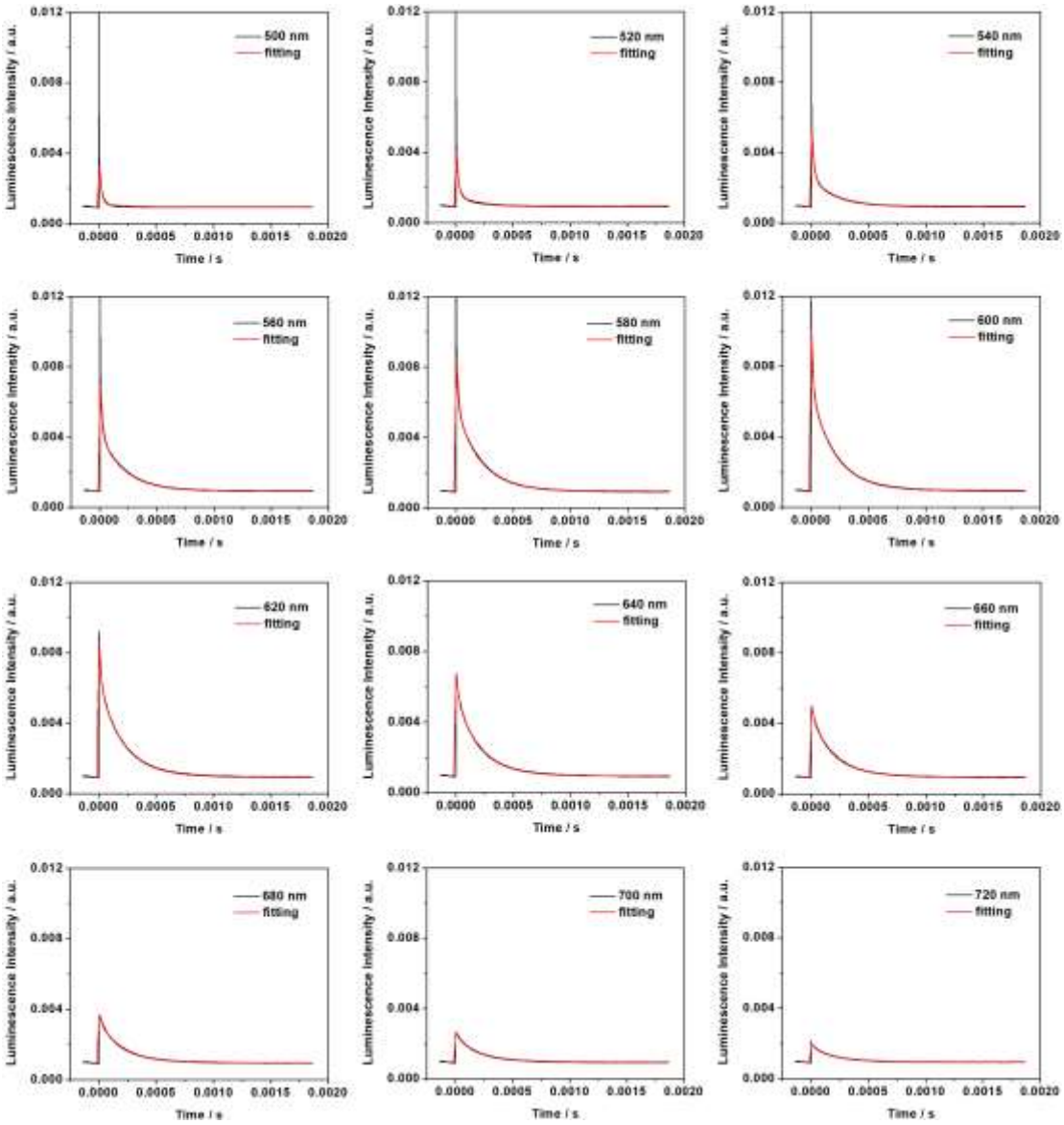

Figure S22. Luminescence decay traces and obtained by the ns-ms time-resolved luminescence technique the corresponding fittings to a multi-exponential decay for $Ag_1Li_3Na_8$-LTA, at 298 K in a 2-ms time window (λ_{ex}=265 nm, λ_{det}=500-720 nm).

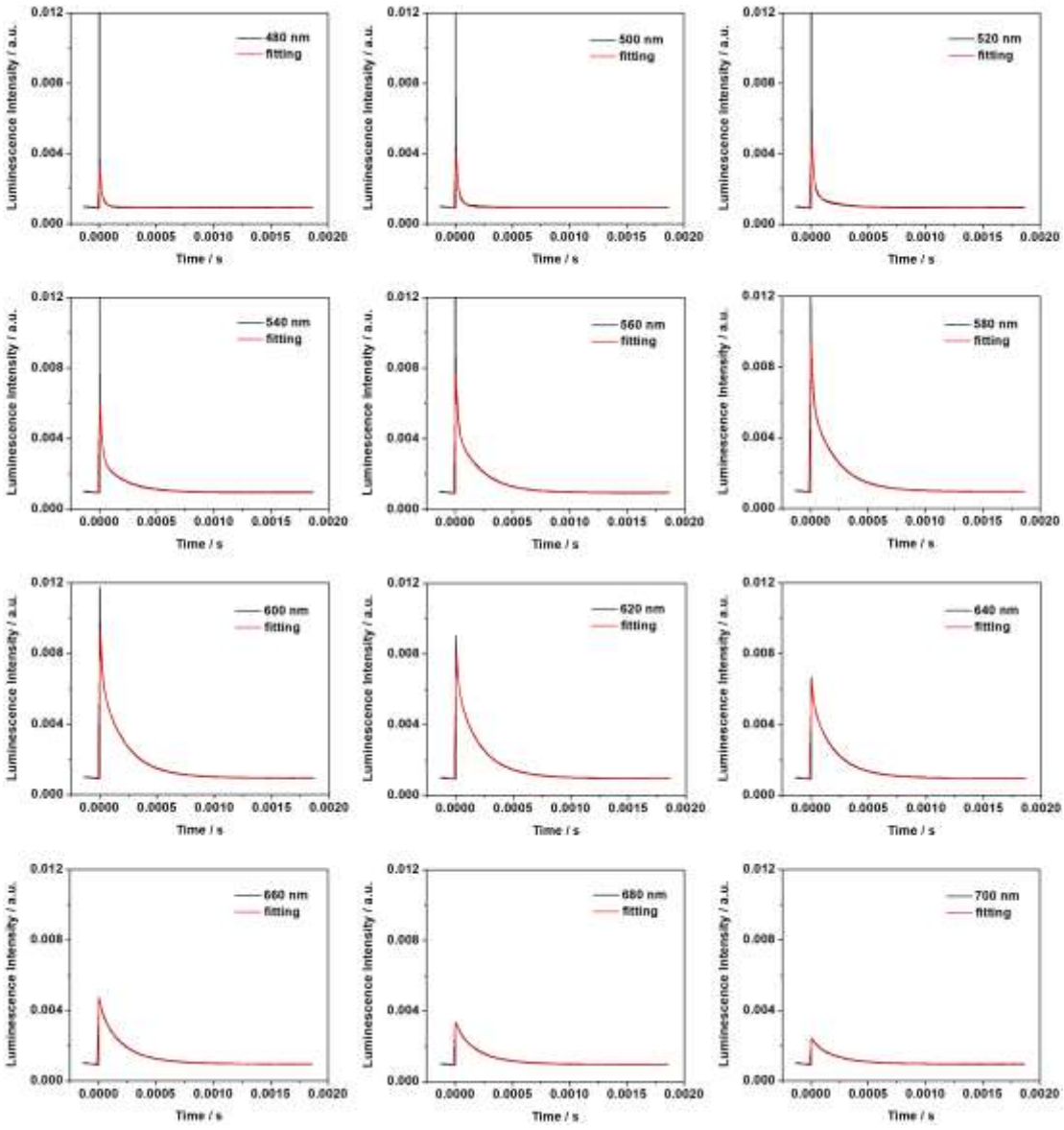

Figure S23. Luminescence decay traces obtained by the ns-ms time-resolved luminescence technique and the corresponding fittings to a multi-exponential decay for $Ag_1Li_4Na_7$-LTA, at 298 K in a 2-ms time window (λ_{ex}=265 nm, λ_{det}=480-700 nm).

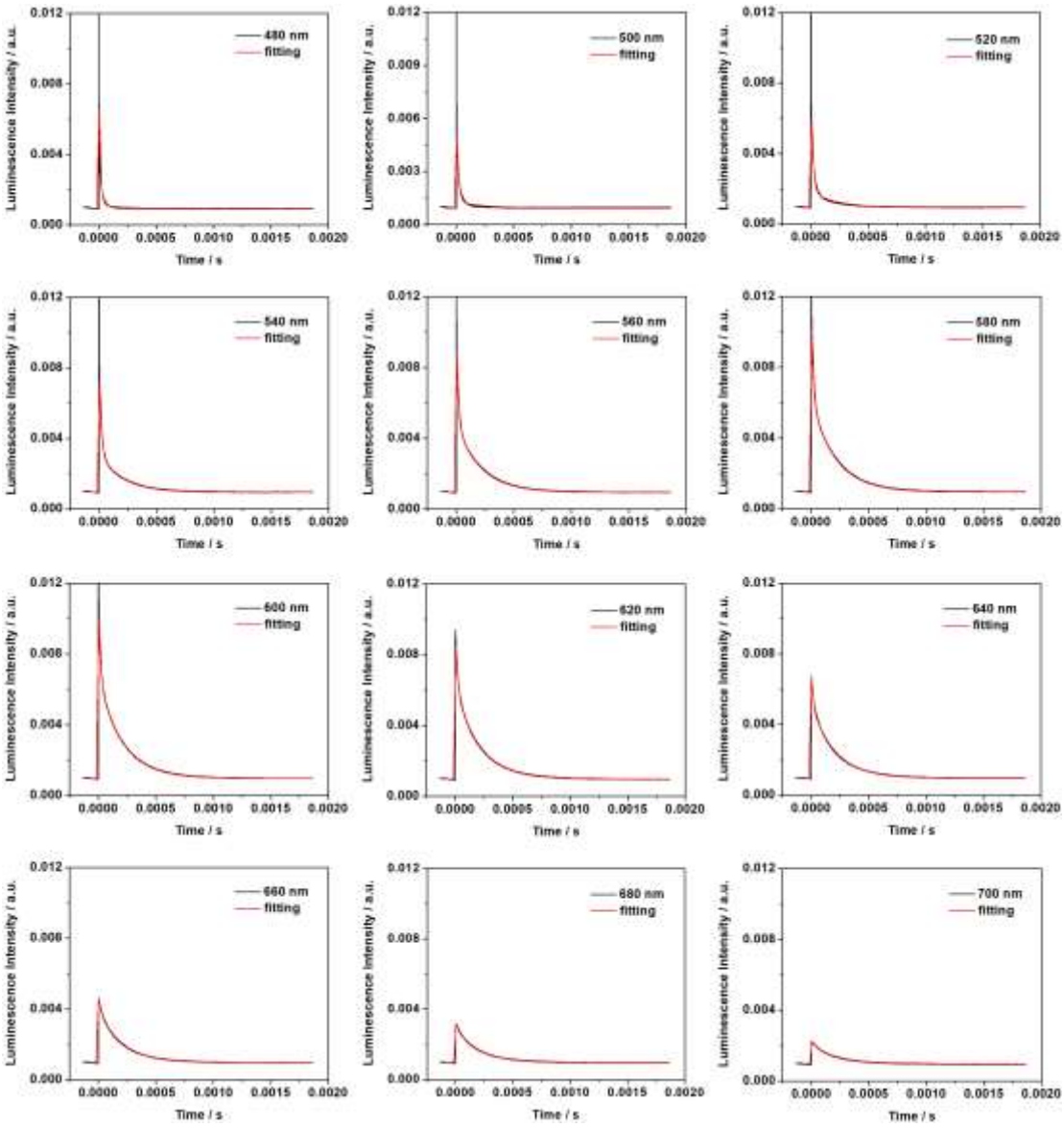

Figure S24. Luminescence decay traces obtained by the ns-ms time-resolved luminescence technique and the corresponding fittings to a multi-exponential decay for $Ag_1Li_5Na_6$-LTA, at 298 K in a 2-ms time window (λ_{ex}=265 nm, λ_{det}=480-700 nm).

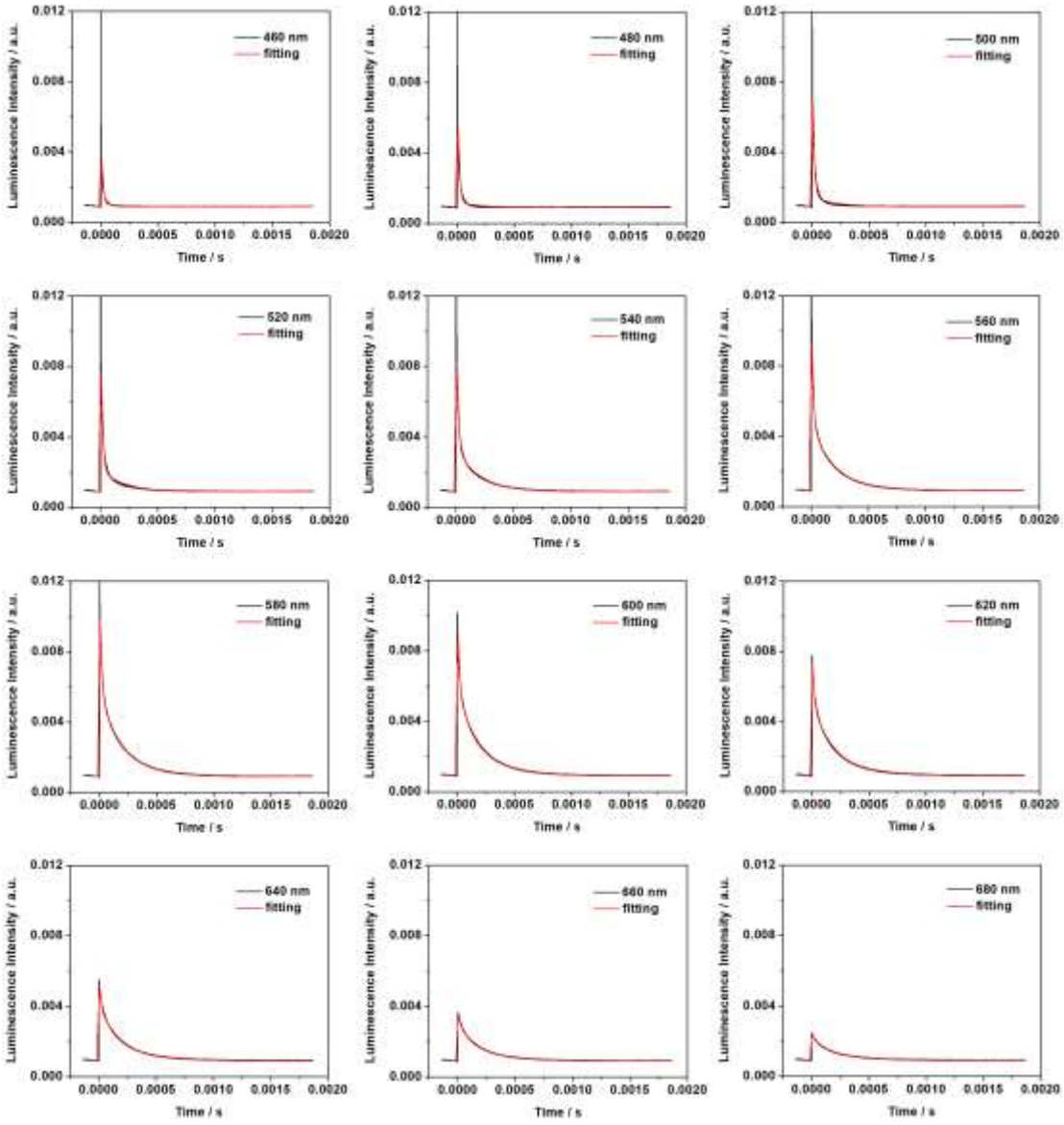

Figure S25. Luminescence decay traces obtained by the ns-ms time-resolved luminescence technique and the corresponding fittings to a multi-exponential decay for $Ag_1Li_7Na_4$-LTA, at 298 K in a 2-ms time window (λ_{ex}=265 nm, λ_{det}=460-680 nm).

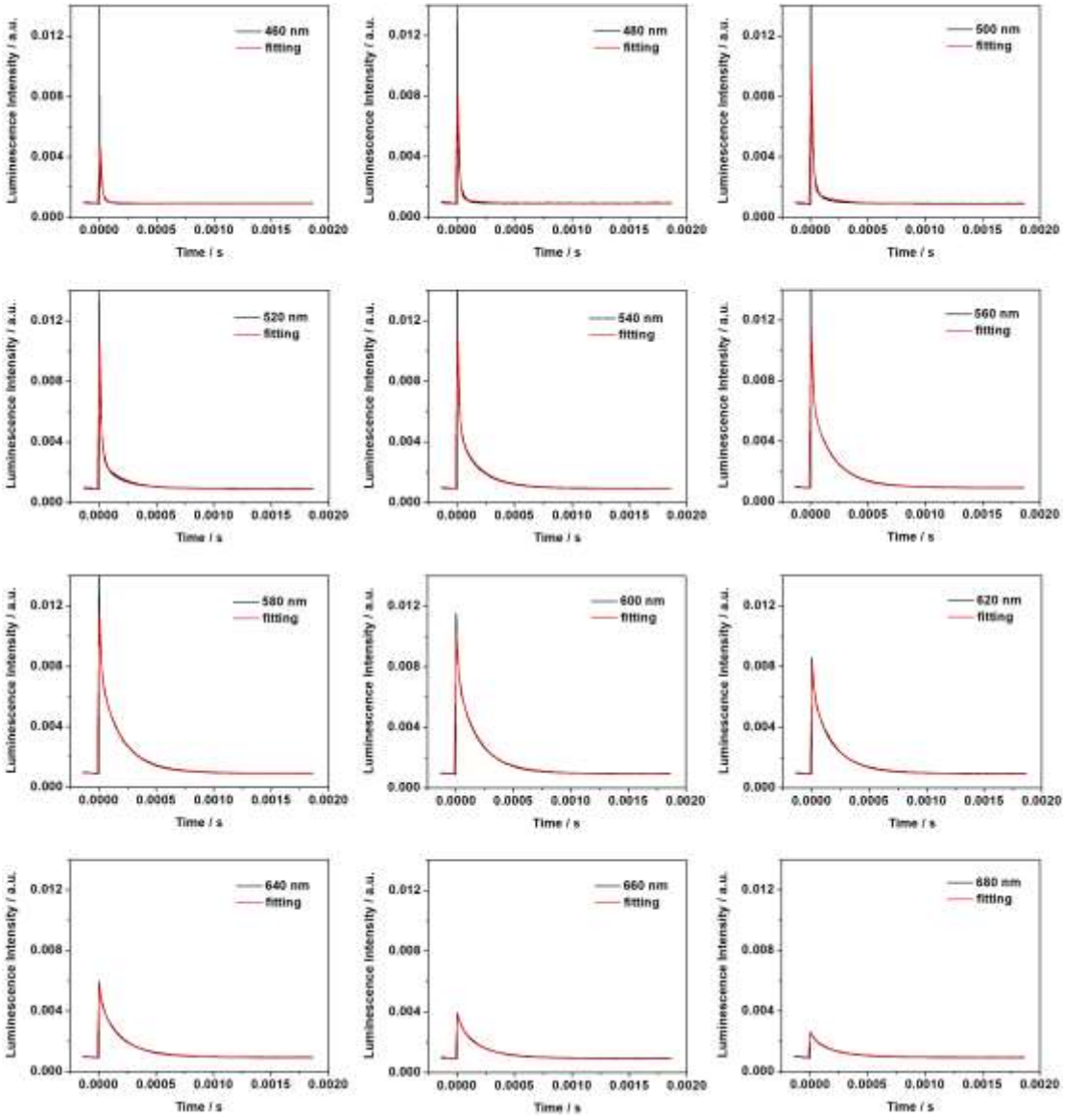

Figure S26. Luminescence decay traces obtained by the ns-ms time-resolved luminescence technique and the corresponding fittings to a multi-exponential decay for $Ag_1Li_8Na_3$-LTA, at 298 K in a 2-ms time window (λ_{ex}=265 nm, λ_{det}=460-680 nm).

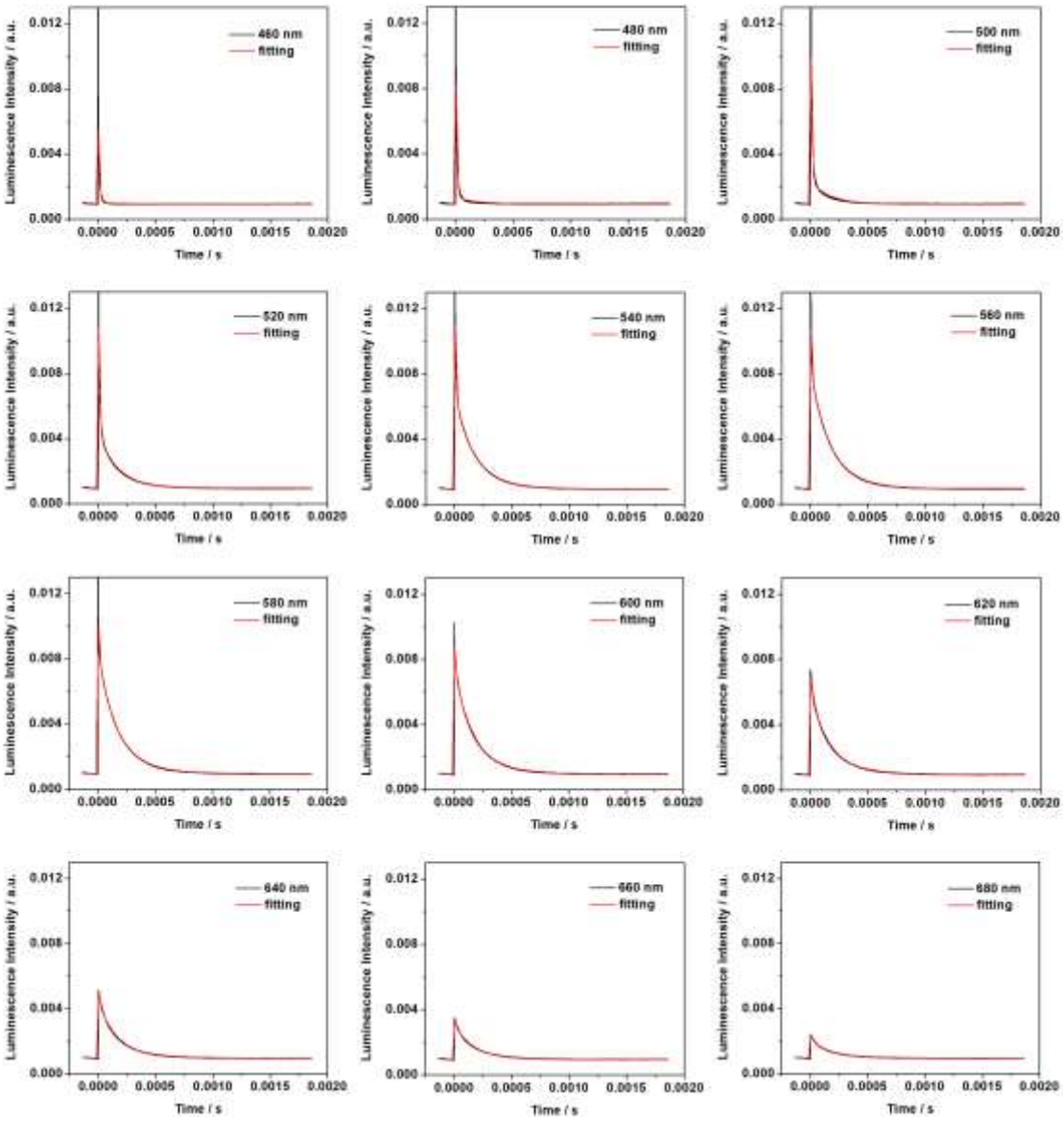

Figure S27. Luminescence decay traces obtained by the ns-ms time-resolved luminescence technique and the corresponding fittings to a multi-exponential decay for $Ag_1Li_9Na_2$-LTA, at 298 K in a 2-ms time window (λ_{ex}=265 nm, λ_{det}=460-680 nm).

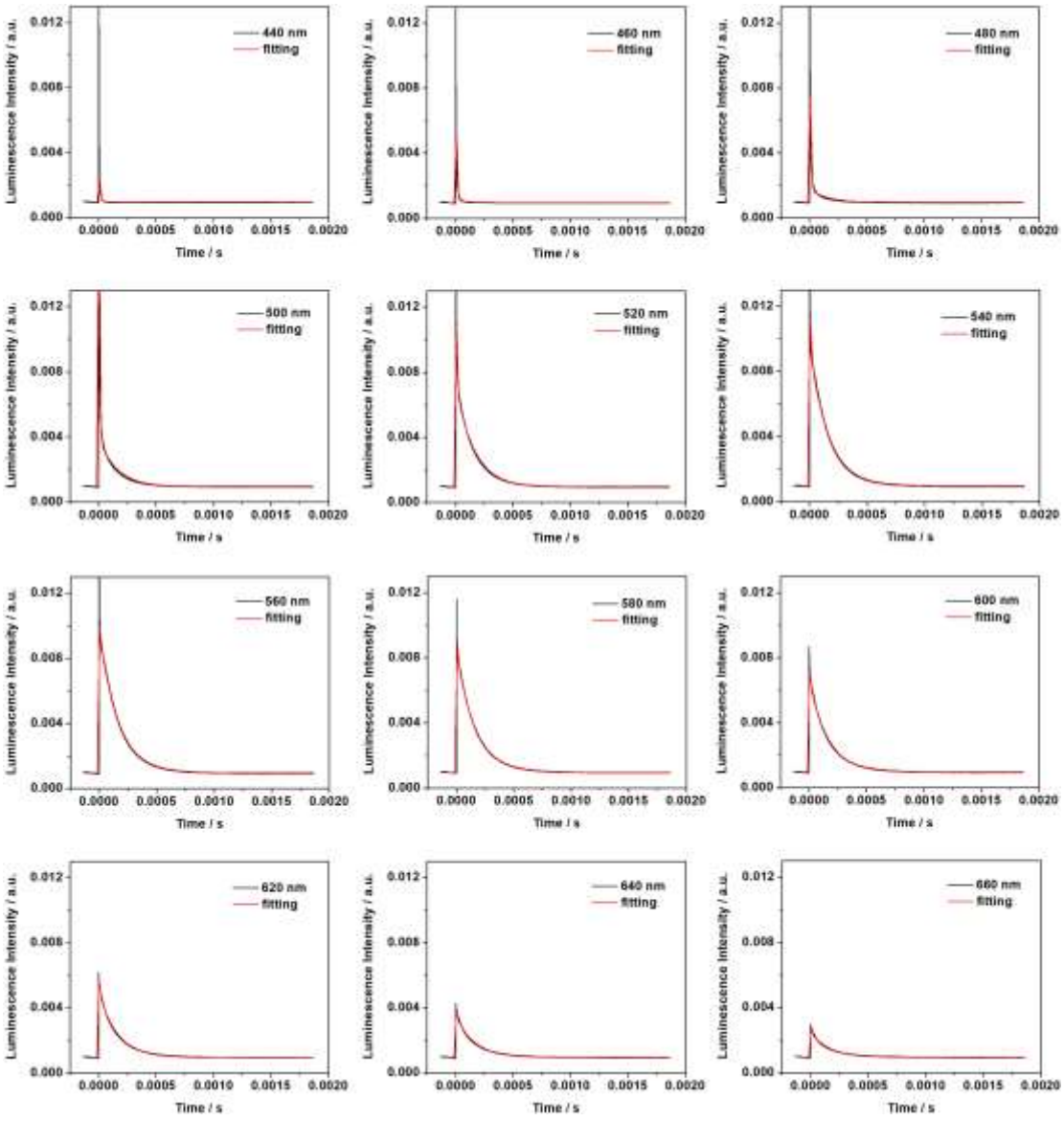

Figure S28. Luminescence decay traces obtained by the ns-ms time-resolved luminescence technique and the corresponding fittings to a multi-exponential decay for $Ag_1Li_{10}Na_1$-LTA, at 298 K in a 2-ms time window (λ_{ex}=265 nm, λ_{det}=440-660 nm).

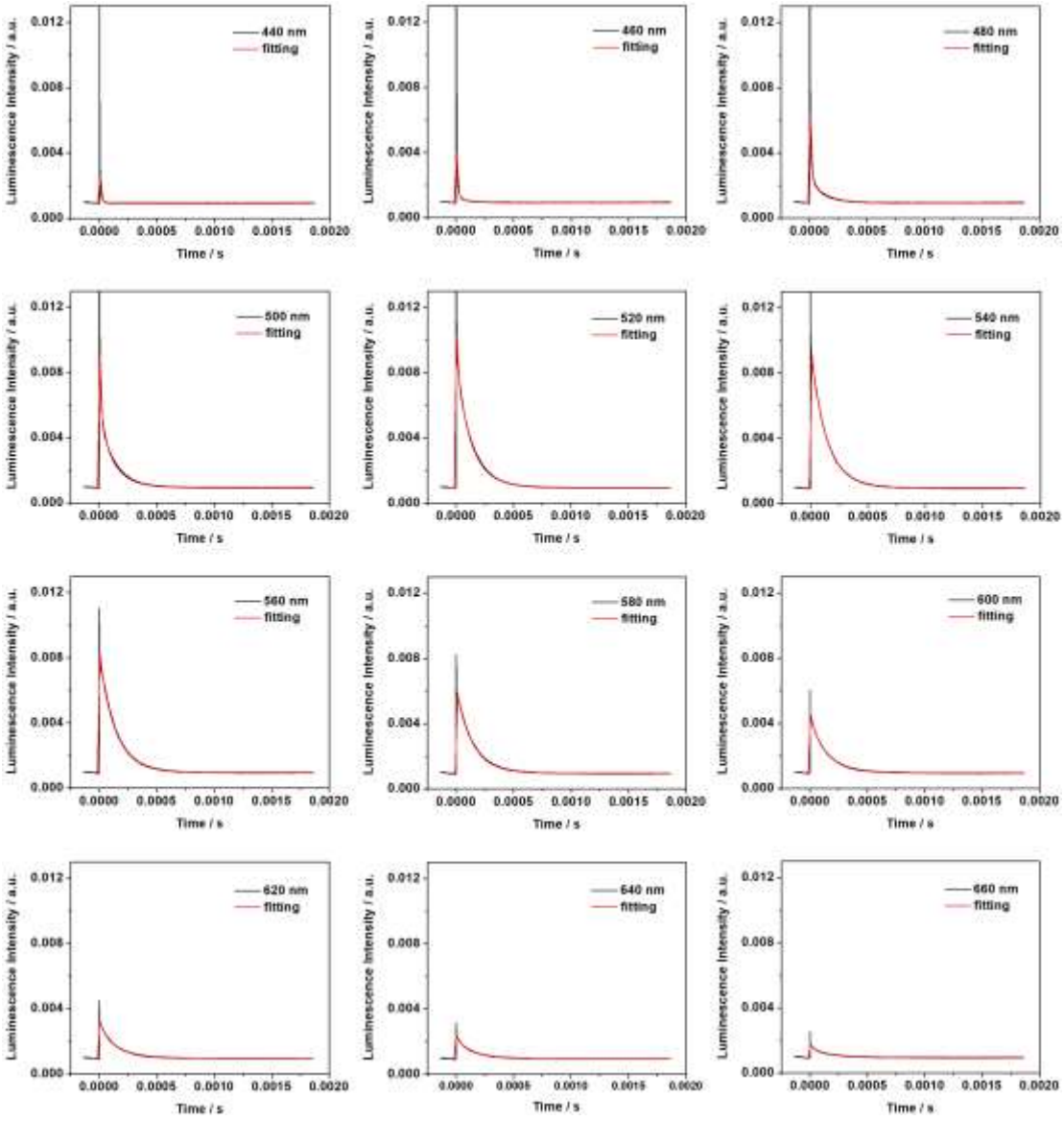

Figure S29. Luminescence decay traces obtained by the ns-ms time-resolved luminescence technique and the corresponding fittings to a multi-exponential decay for $Ag_1Li_{11}Na_0$-LTA, at 298 K in a 2-ms time window (λ_{ex}=265 nm, λ_{det}=440-660 nm).

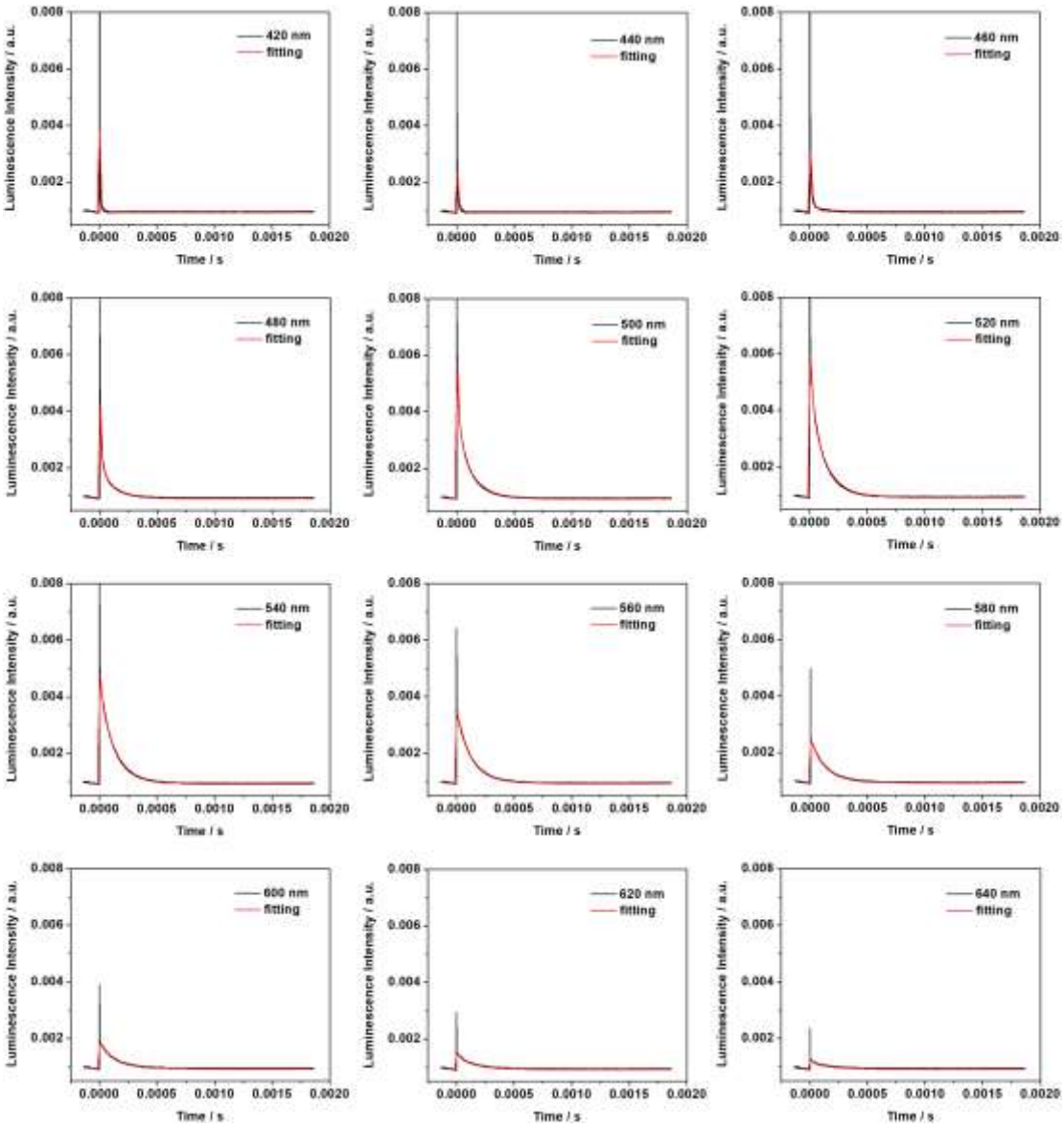

Figure S30. Luminescence decay traces obtained by the ns-ms time-resolved luminescence technique and the corresponding fittings to a multi-exponential decay for Ag_1Li_{11}-LTA, at 298 K in a 2-ms time window (λ_{ex}=265 nm, λ_{det}=420-640 nm).

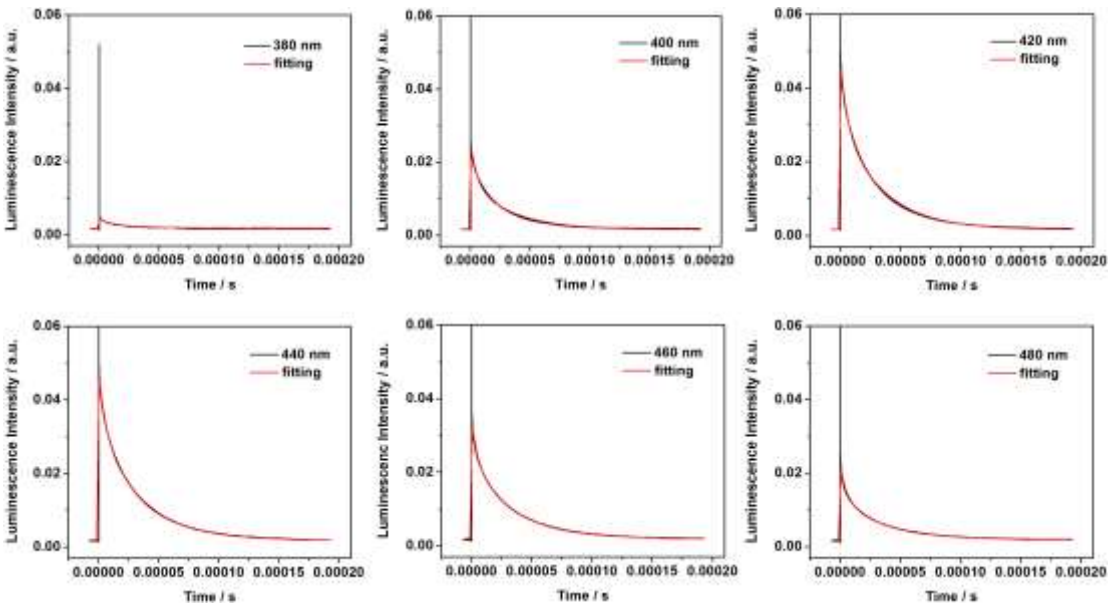

Figure S31. Luminescence decay traces obtained by the ns-ms time-resolved luminescence technique and the corresponding fittings to a multi-exponential decay for $Ag_1Li_0Na_{11}$-LTA, at 77 K in a 200-μs time window (λ_{ex}=265 nm, λ_{det}=380-480 nm).

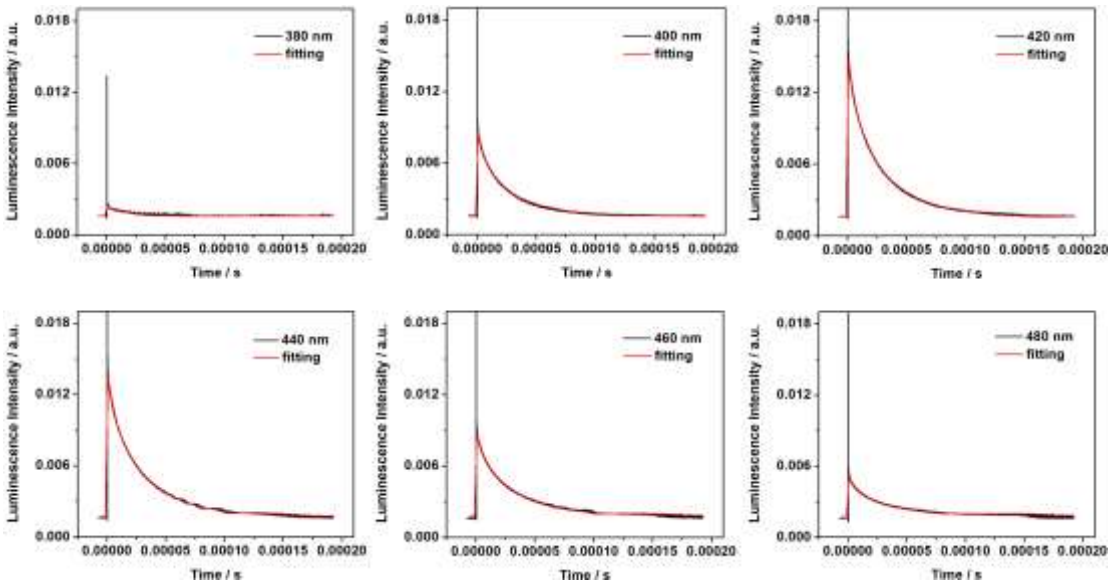

Figure S32. Luminescence decay traces obtained by the ns-ms time-resolved luminescence technique and the corresponding fittings to a multi-exponential decay for $Ag_1Li_1Na_{10}$-LTA, at 77 K in a 200-μs time window (λ_{ex}=265 nm, λ_{det}=380-480 nm).

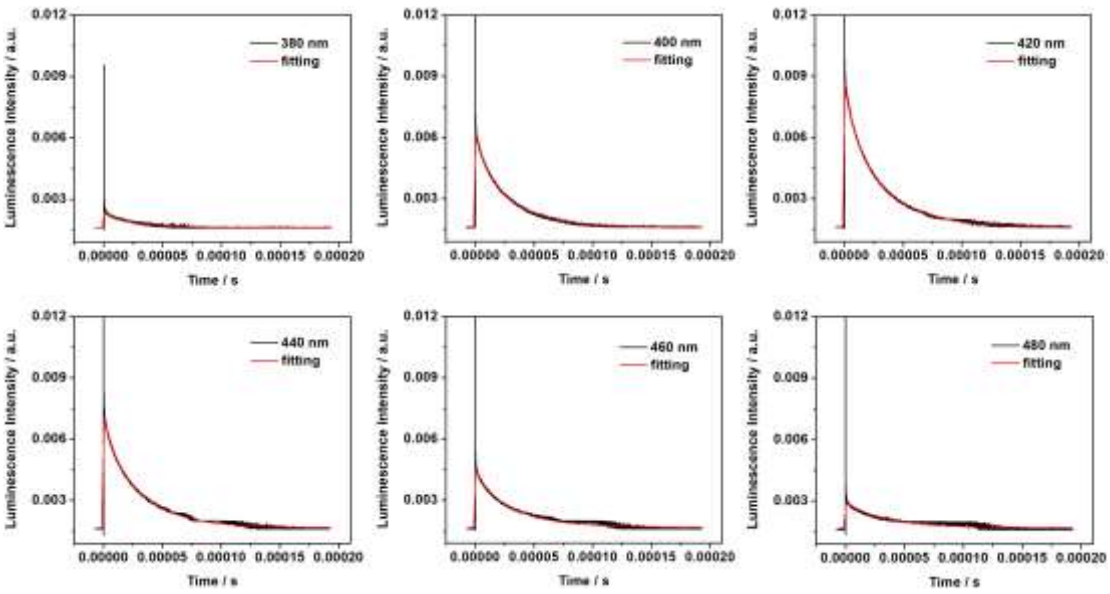

Figure S33. Luminescence decay traces obtained by the ns-ms time-resolved luminescence technique and the corresponding fittings to a multi-exponential decay for $Ag_1Li_2Na_9$-LTA, at 77 K in a 200-μs time window (λ_{ex}=265 nm, λ_{det}=380-480 nm).

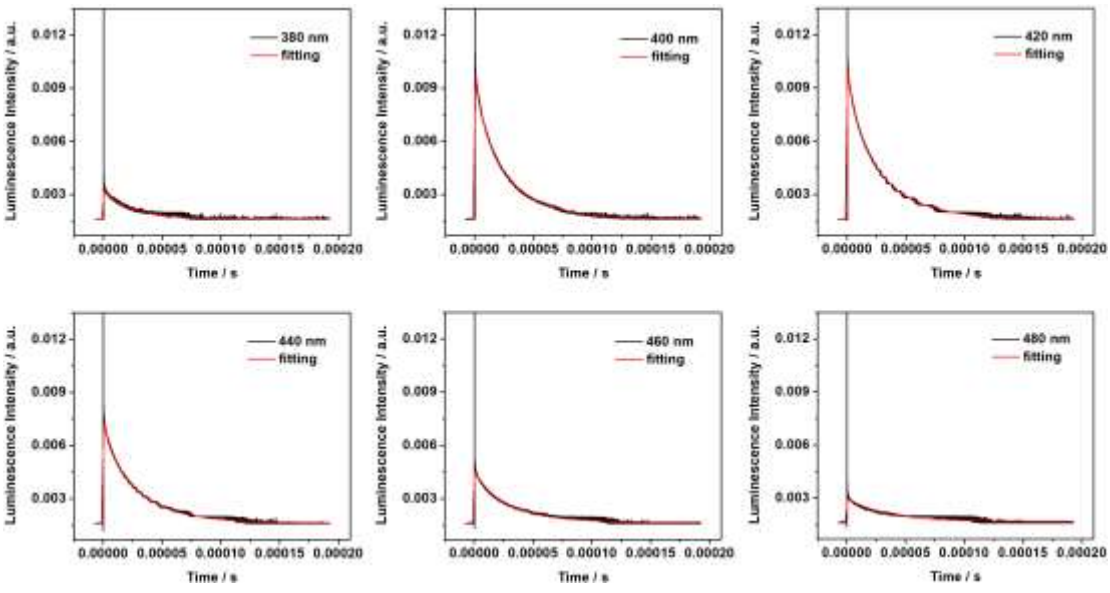

Figure S34. Luminescence decay traces obtained by the ns-ms time-resolved luminescence technique and the corresponding fittings to a multi-exponential decay for $Ag_1Li_3Na_8$-LTA, at 77 K in a 200-μs time window (λ_{ex}=265 nm, λ_{det}=380-480 nm).

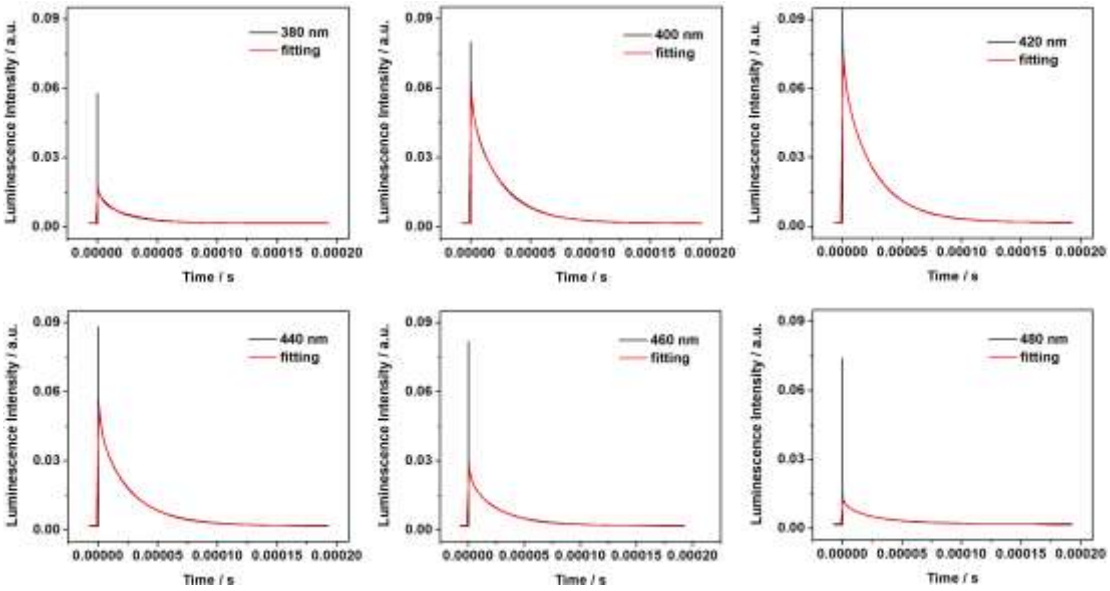

Figure S35. Luminescence decay traces obtained by the ns-ms time-resolved luminescence technique and the corresponding fittings to a multi-exponential decay for $Ag_1Li_4Na_7$-LTA, at 77 K in a 200-μs time window (λ_{ex}=265 nm, λ_{det}=380-480 nm).

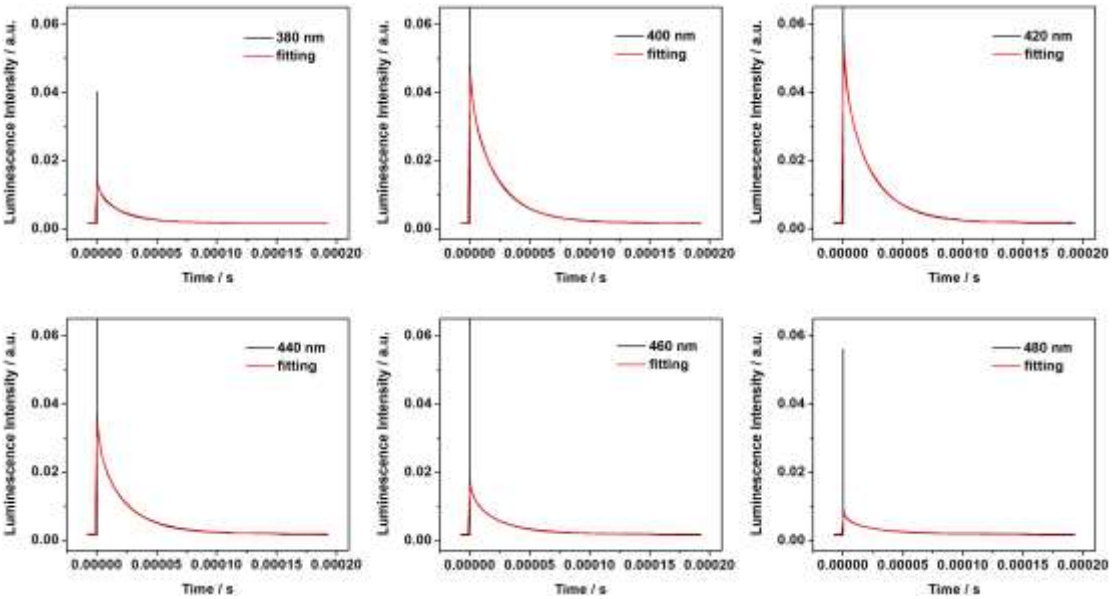

Figure S36. Luminescence decay traces obtained by the ns-ms time-resolved luminescence technique and the corresponding fittings to a multi-exponential decay for $Ag_1Li_5Na_6$-LTA, at 77 K in a 200-μs time window (λ_{ex}=265 nm, λ_{det}=380-480 nm).

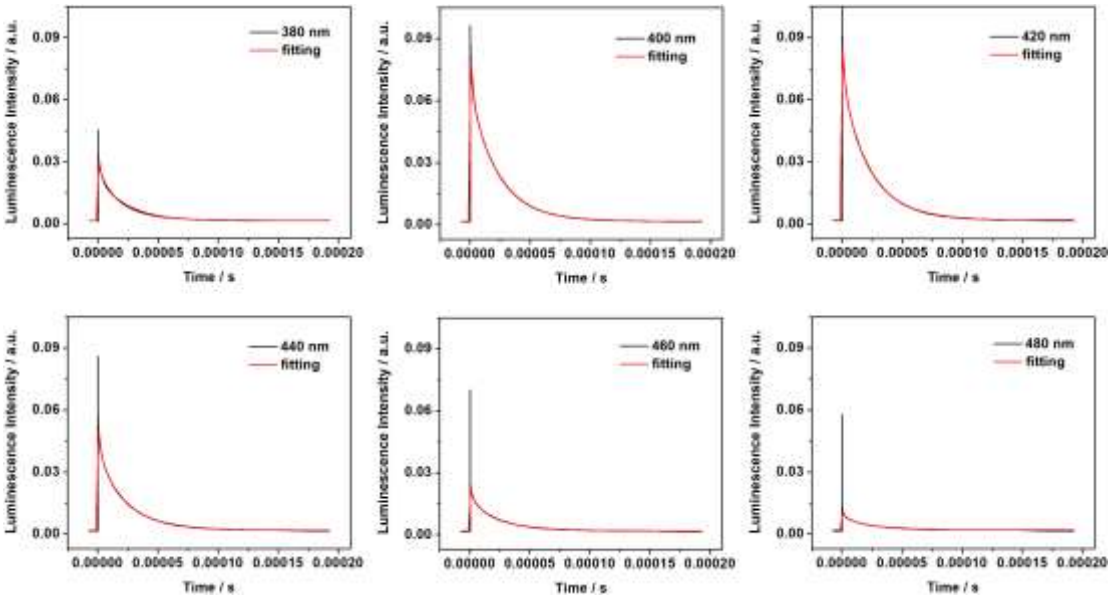

Figure S37. Luminescence decay traces obtained by the ns-ms time-resolved luminescence technique and the corresponding fittings to a multi-exponential decay for $Ag_1Li_7Na_4$-LTA, at 77 K in a 200-μs time window (λ_{ex}=265 nm, λ_{det}=380-480 nm).

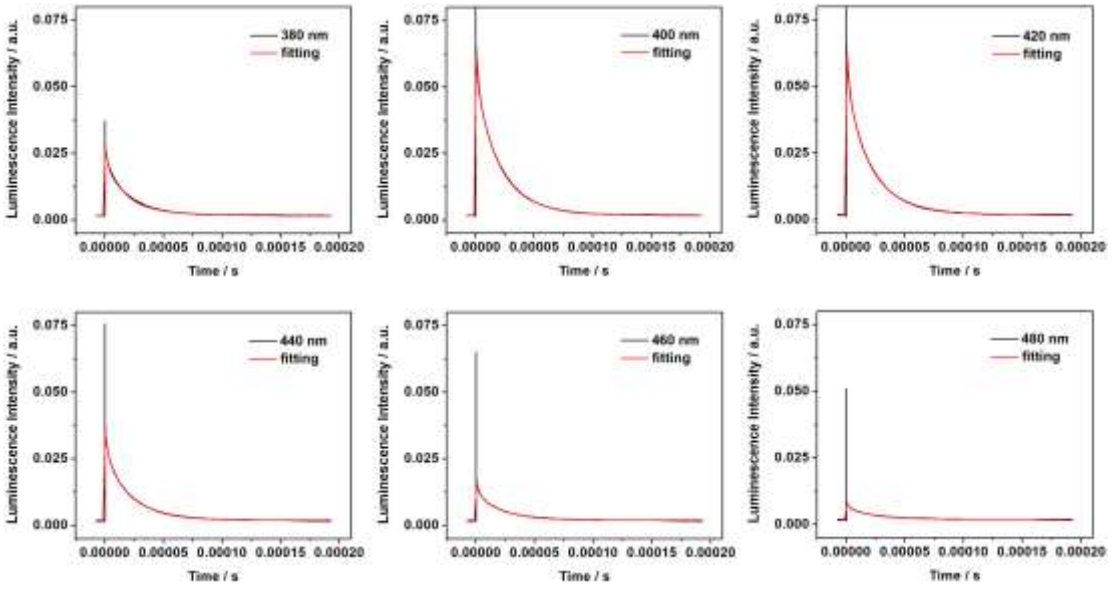

Figure S38. Luminescence decay traces obtained by the ns-ms time-resolved luminescence technique and the corresponding fittings to a multi-exponential decay for $Ag_1Li_8Na_3$-LTA, at 77 K in a 200-μs time window (λ_{ex}=265 nm, λ_{det}=380-480 nm).

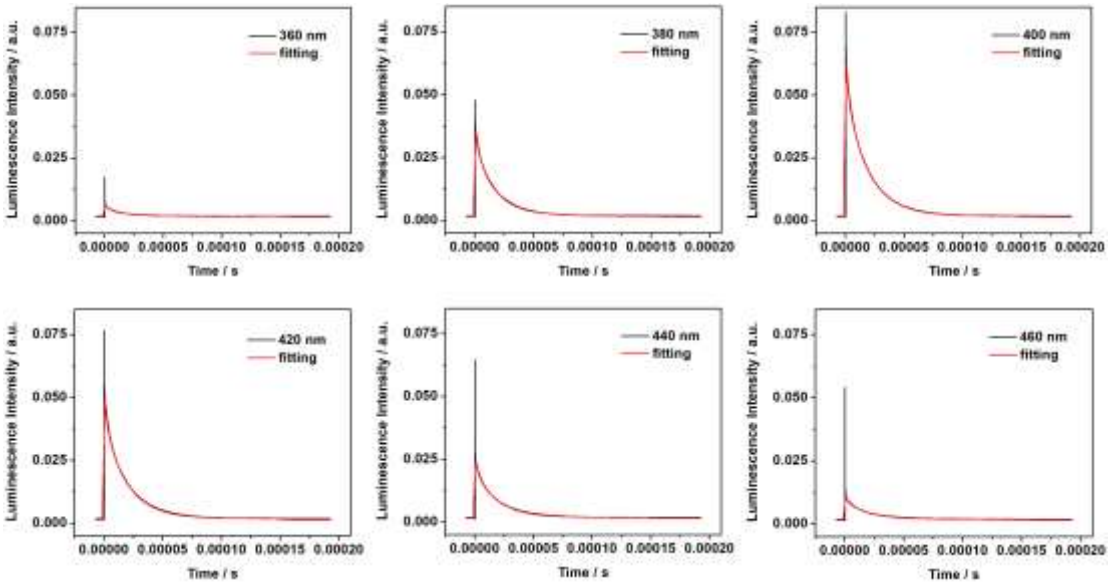

Figure S39. Luminescence decay traces obtained by the ns-ms time-resolved luminescence technique and the corresponding fittings to a multi-exponential decay for $Ag_1Li_9Na_2$-LTA, at 77 K in a 200-μs time window (λ_{ex}=265 nm, λ_{det}=360-460 nm).

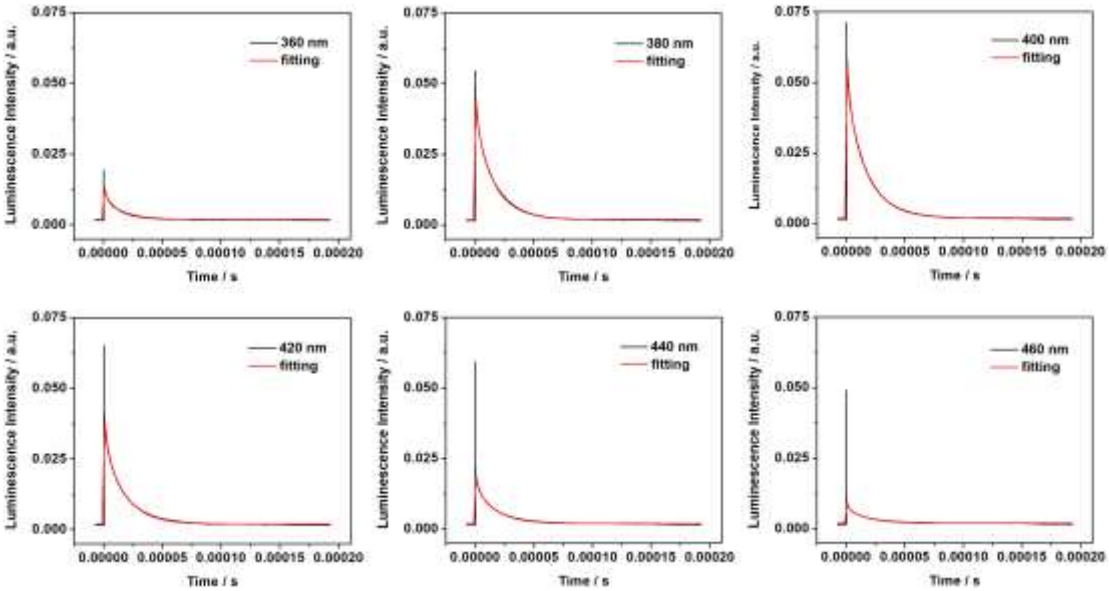

Figure S40. Luminescence decay traces obtained by the ns-ms time-resolved luminescence technique and the corresponding fittings to a multi-exponential decay for $Ag_1Li_{10}Na_1$-LTA, at 77 K in a 200-μs time window (λ_{ex}=265 nm, λ_{det}=360-460 nm).

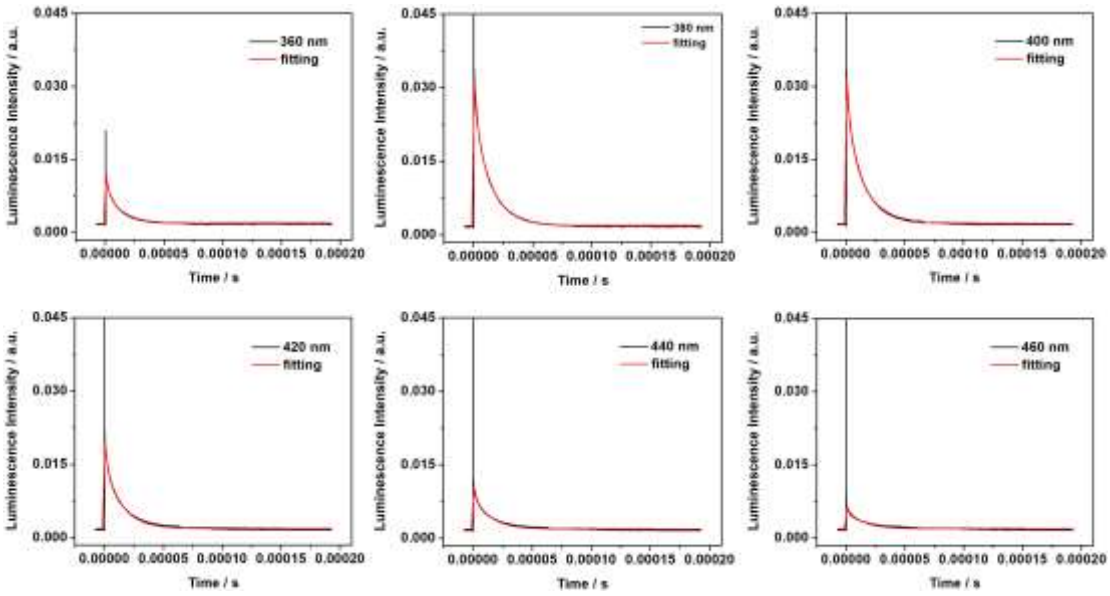

Figure S41. Luminescence decay traces obtained by the ns-ms time-resolved luminescence technique and the corresponding fittings to a multi-exponential decay for $Ag_1Li_{11}Na_0$-LTA, at 77 K in a 200-μs time window (λ_{ex}=265 nm, λ_{det}=360-460 nm).

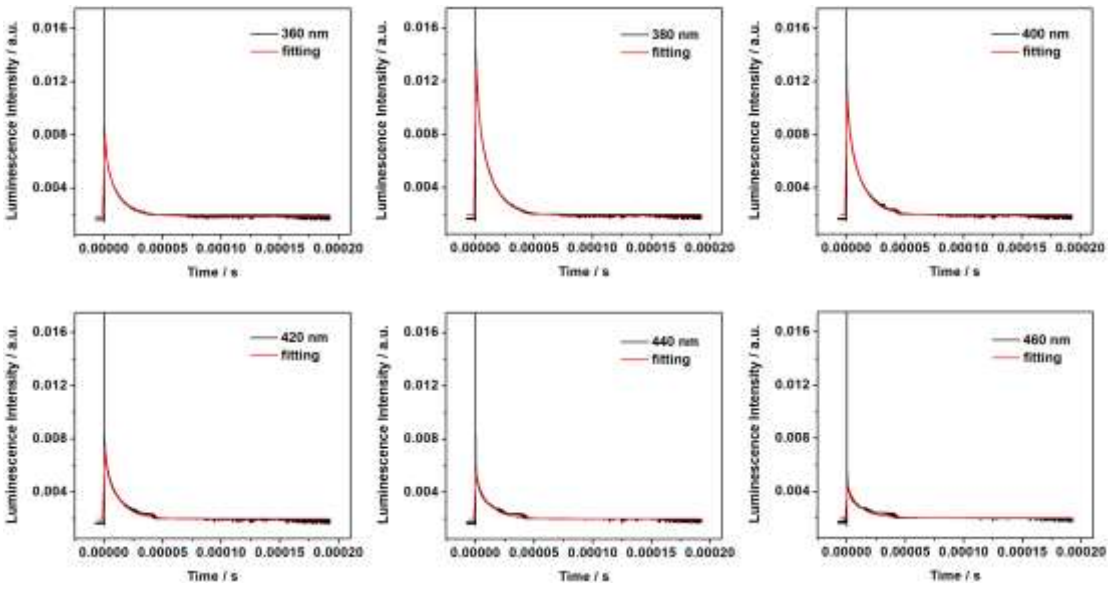

Figure S42. Luminescence decay traces obtained by the ns-ms time-resolved luminescence technique and the corresponding fittings to a multi-exponential decay for Ag_1Li_{11}-LTA, at 77 K in a 200-μs time window (λ_{ex}=265 nm, λ_{det}=360-460 nm).

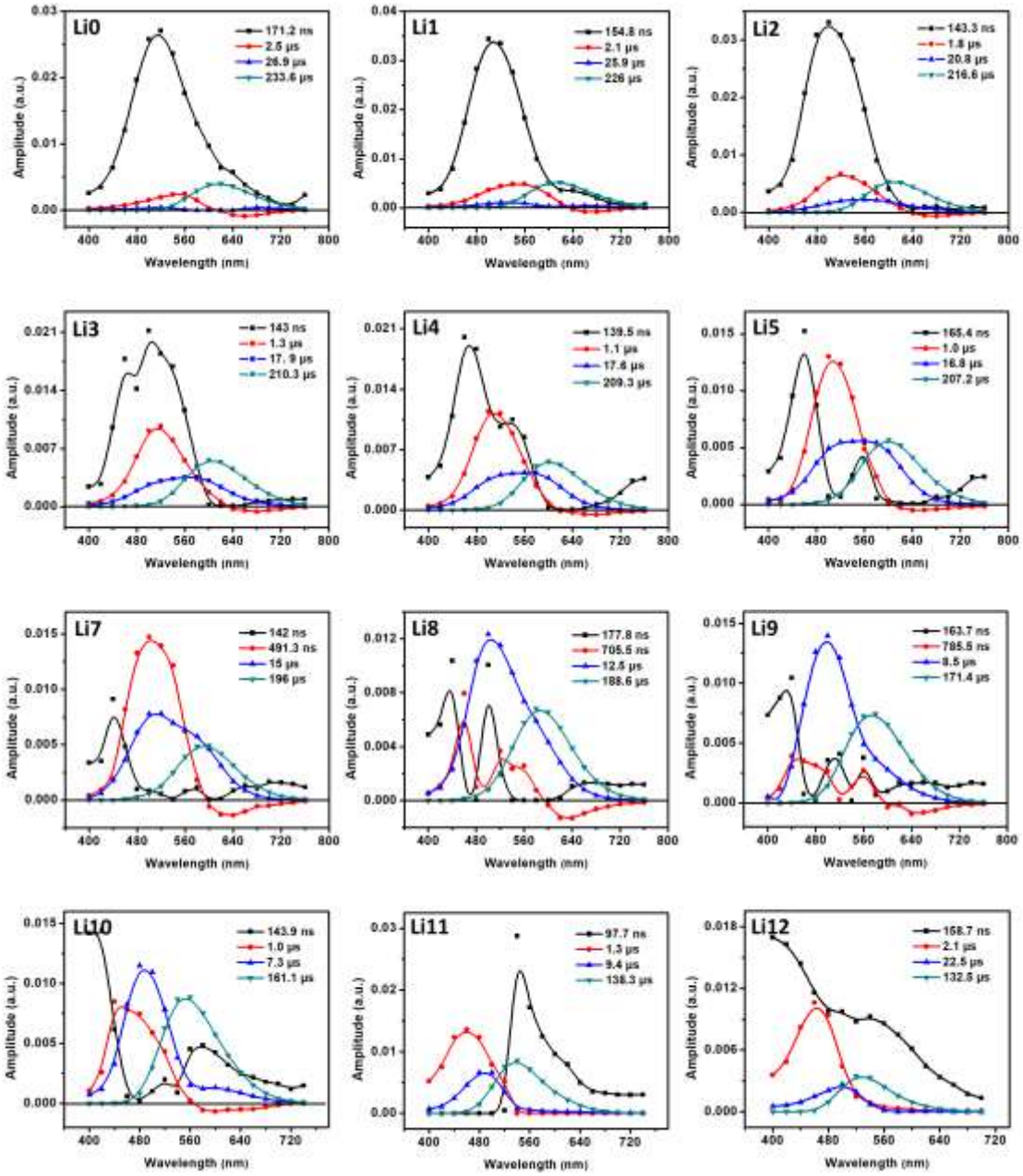

Figure S43. The amplitude-to-wavelength dependence (AWD) of the different decay components obtained by the ns-ms time-resolved luminescence technique for Ag_1-exchanged Li_xNa_{12-x}-LTA (x=0-12), at 298 K in a 2-ms time window (λ_{ex}=265 nm, λ_{det}=400-760 nm).

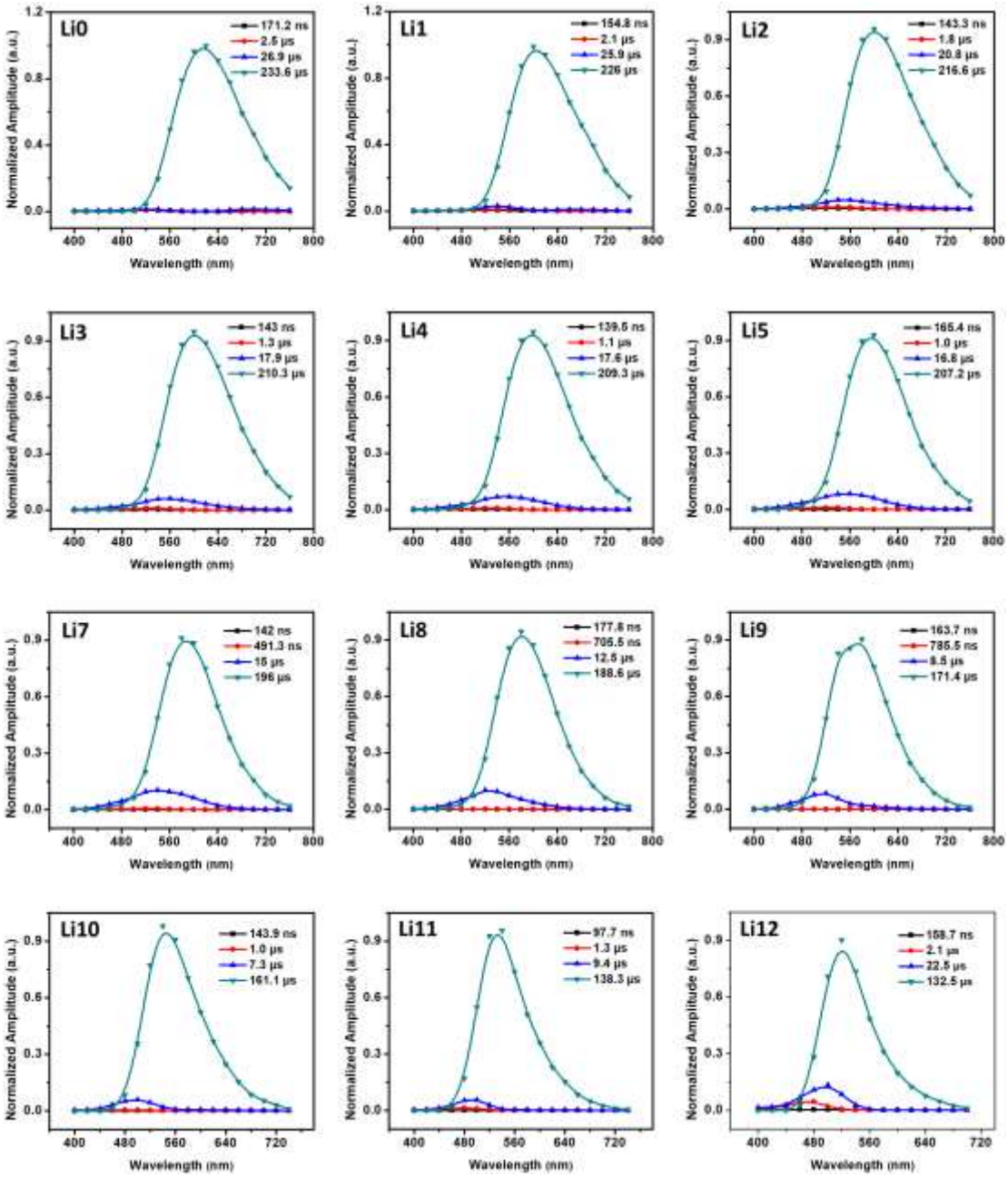

Figure S44. The decay associated spectra (DAS) of the different decay components obtained by the ns-ms time-resolved luminescence technique for Ag_1-exchanged Li_xNa_{12-x}-LTA (x=0-12), at 298 K in a 2-ms time window (λ_{ex}=265 nm, λ_{det}=400-760 nm).

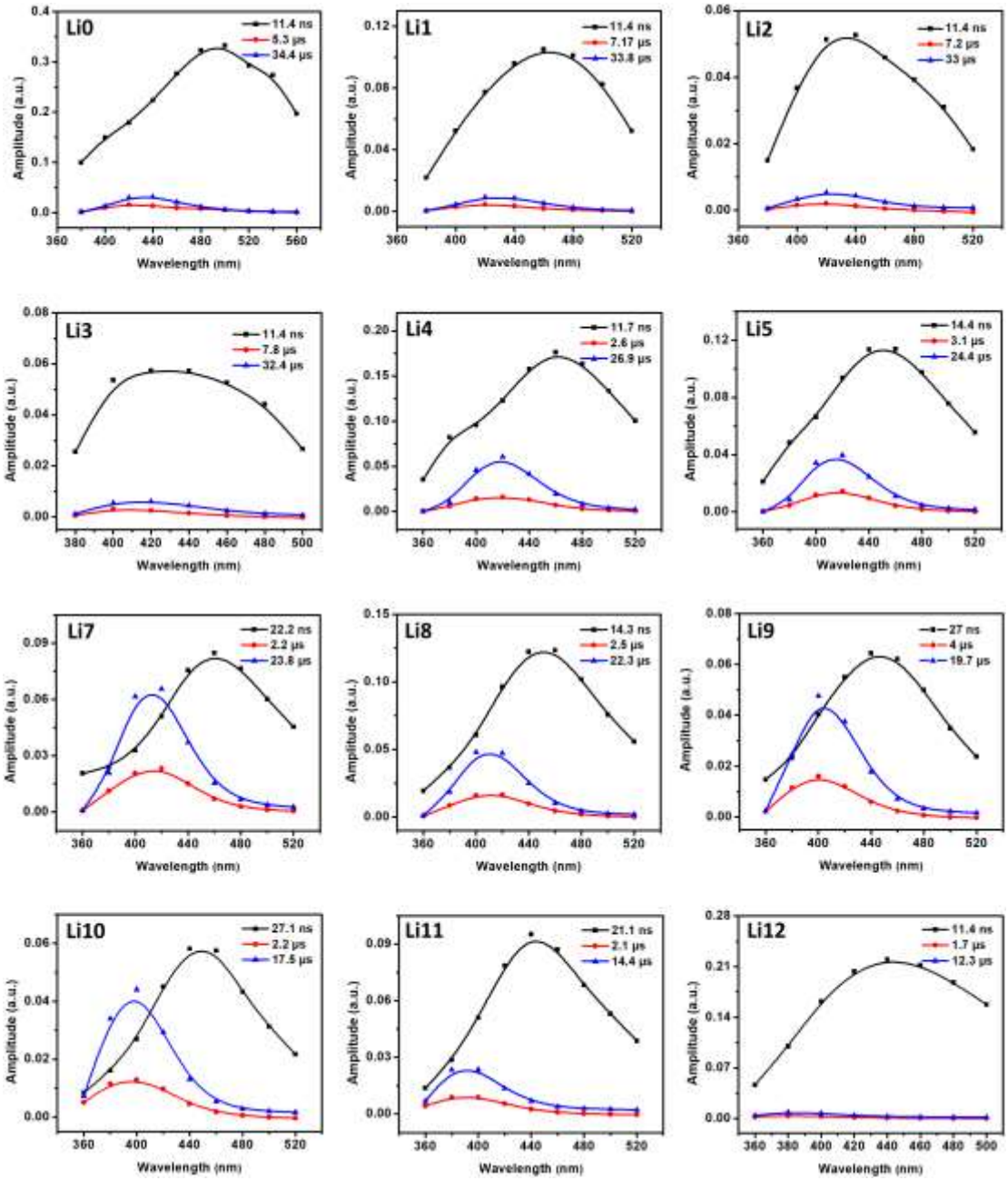

Figure S45. The amplitude-to-wavelength dependence (AWD) of the different decay components obtained by the ns-ms time-resolved luminescence technique for Ag_1-exchanged Li_xNa_{12-x}-LTA (x=0-12), at 77 K in a 200-µs time window (λ_{ex}=265 nm, λ_{det}=360-560 nm).

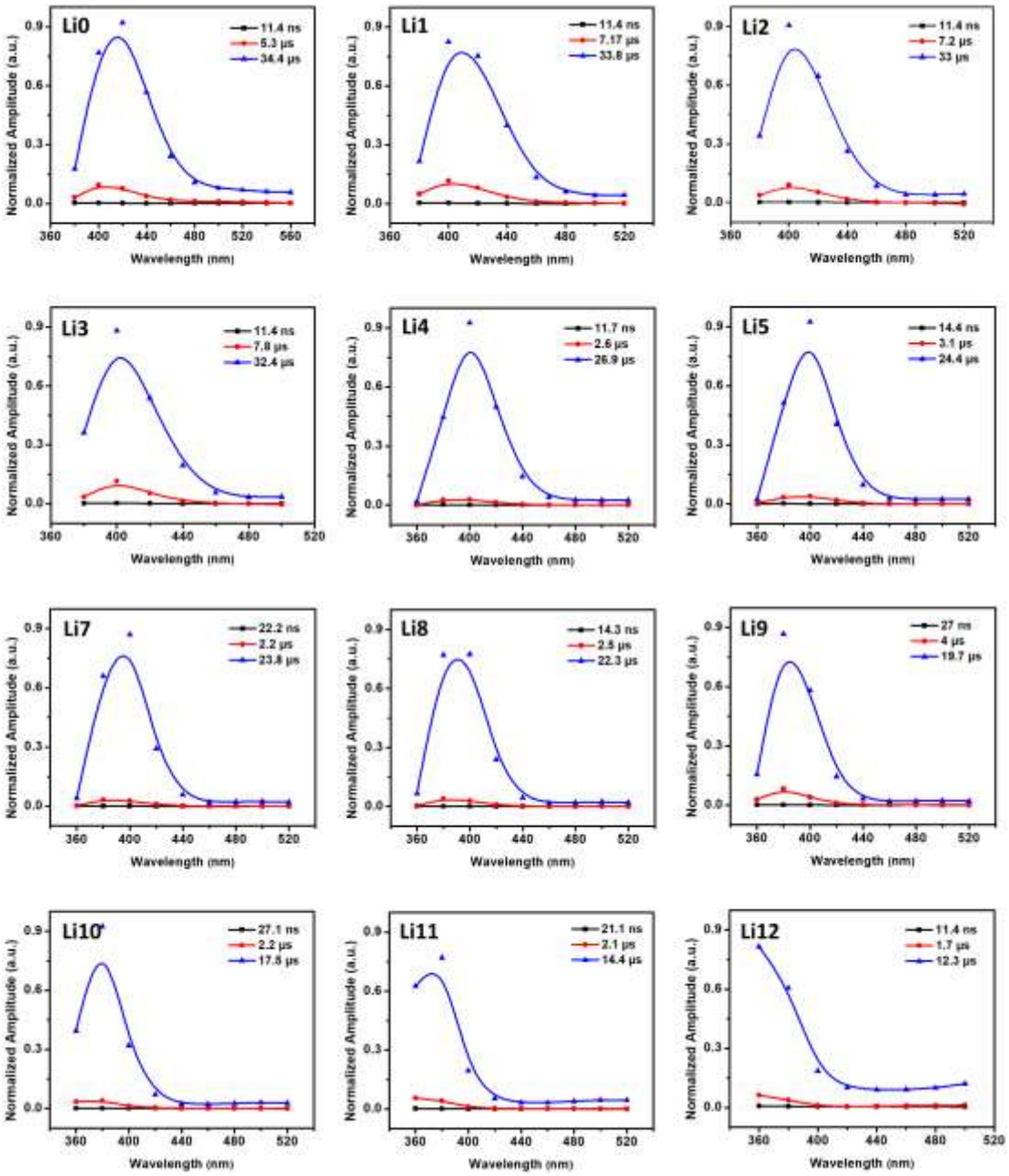

Figure S46. The decay associated spectra (DAS) of the different decay components obtained by the ns-ms time-resolved luminescence technique for Ag_1-exchanged Li_xNa_{12-x}-LTA (x=0-12), at 77 K in a 200-µs time window (λ_{ex}=265 nm, λ_{det}=360-560 nm).

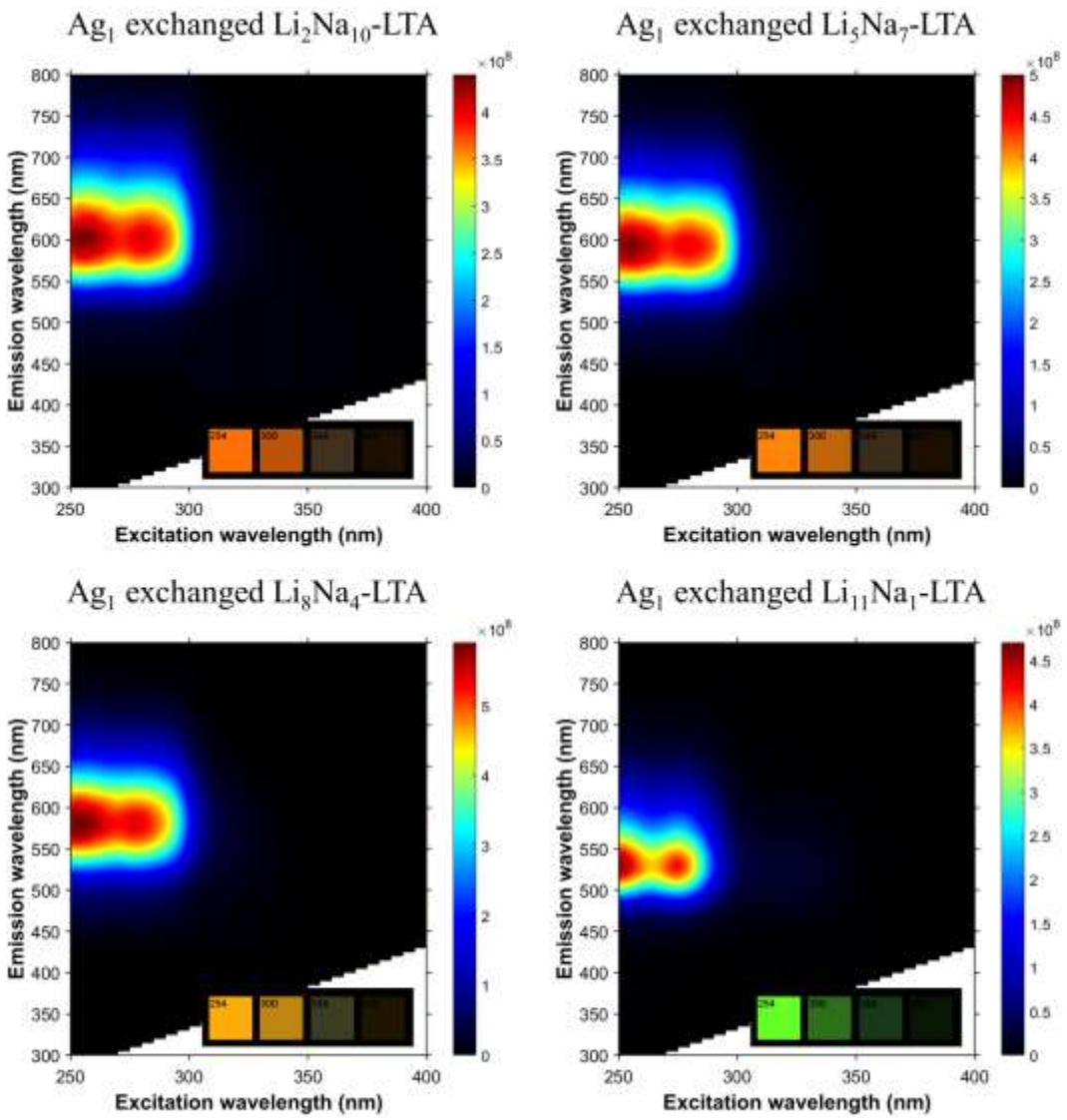

Figure S47. The re-checked two-dimensional excitation/emission plots of hydrated Ag_1-exchanged Li_xNa_{12-x}-LTA (x=2, 5, 8, 11) samples at 298 K after the measurements of the low temperature PL and time-resolved luminescence.

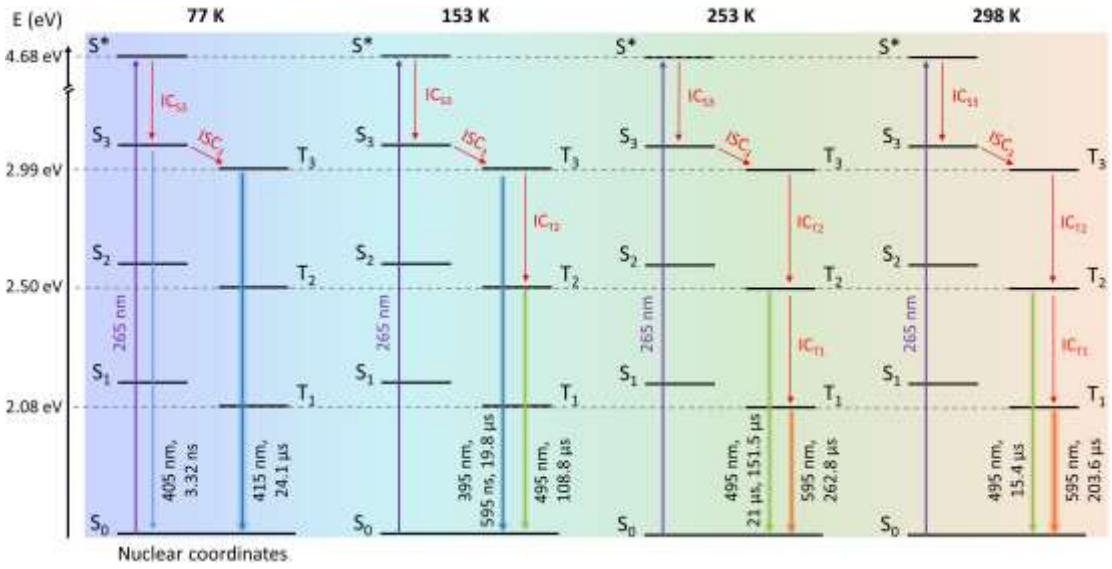

Figure S48. Simplified version of the proposed kinetic scheme of the processes observed upon excitation of $Ag_1Li_6Na_5LTA$ at the specified temperatures (λ_{ex}=265 nm) assuming that the internal conversion occurs only between the different triplet states. As discussed in main text, this kinetic model is based on relaxation by internal conversation between triplet states (IC_T) together with geometry changes of AgCLs. These geometry changes require to overcome the energy barrier between the different triplet excited states by thermal activation.

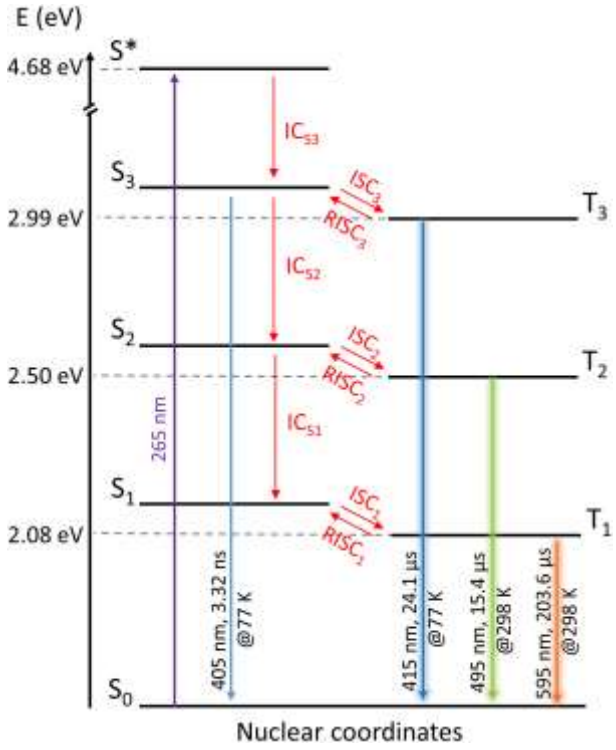

Figure S49. Simplified version of the proposed kinetic scheme of the processes observed upon excitation of $Ag_1Li_6Na_5LTA$ as the function of temperature (λ_{ex}=265 nm) assuming that the internal conversion occurs only between the different singlet states. As another possibility of the interconversion by overcoming the observed barrier, this scheme requires RISC from triplet to singlet excited states under thermal activation.

The long decay times of the main emission components suggest that the emitting species is always populated through a triplet state. This emitting species can be either the triplet state or a singlet state in equilibrium with a triplet state. In the latter case an equilibrium between singlet and triplet states is established by a combination of intersystem crossing and reverse intersystem crossing characterized by the rate constants k_{ISC} and k_{RISC}. The establishment of this equilibrium would require that $k_{T3\text{-}S0}+k_{ICT2}<k_{RISC3}$ (or $k_{T2\text{-}S0}+k_{ICT1}<k_{RISC2}$ or $k_{T1\text{-}S0}<k_{RISC1}$).

Contrary to what was concluded for Ag_3Na_9-LTA by Fron et al.,[3] it is unlikely that in the systems reported here, reversible population of traps is responsible for the long decay times. If traps would be involved, it is difficult to see why traps populated from S_3 only yield S_3 on detrapping and not S_2 or S_1. It is difficult to see how each of the three different emitting states would be linked to a specific and different trap.

Hence transition from S_3 to S_2 (or T_3 to T_2) will involve a geometric relaxation, probably associated with an energy barrier as the rate of this conversion is temperature dependent. We can expect that this relaxation and the corresponding barrier are similar for singlet and triplet states. Hence the values of k_{ICT2} and k_{ICS2} (or k_{ICT1} and k_{ICS1}) will be similar. Although both processes are expected to occur with similar rate constant, they will not occur with similar efficiency. As $\tau_{T3}=1/(k_{T3\text{-}S0}+k_{ICT2})$ and $\tau_{S3}=1/(k_{S3\text{-}S0}+k_{ICS2})$, while we expect $k_{ICT2}\approx k_{ICS2}$, $k_{S3\text{-}S0}>k_{T3\text{-}S0}$ leads to $\tau_{S3}<\tau_{T3}$. Consequently, the efficiency of k_{ICT2} (which equals to $k_{ICT2}/(k_{T3\text{-}S0}+k_{ICT2})$) will be much larger than k_{ICS2} (which equals to $k_{ICS2}/(k_{S3\text{-}S0}+k_{ICS2})$), which means that the geometric relaxation prefers to take the highly efficient IC_T pathway (the same at higher temperatures as $k_{S2\text{-}S0}$ is also much larger than $k_{T2\text{-}S0}$). Even when the triplets and corresponding singlets are equilibrated and undergo a rapid transition by ISC_3 and $RISC_3$, the concepts discussed above remain valid.

Table S1. Theoretical and measured atomic composition of Ag_1-exchanged Li_xNa_{12-x}-LTA (x=1, 4, 6, 8, 11) and Li fully exchanged LiLTA zeolites for the elements Ag, Li and Na.

Sample	Atomic composition Ag (theoretical)	Atomic composition Ag (measured)	Atomic composition Li (theoretical)	Atomic composition Li (measured)	Atomic composition Na (theoretical)	Atomic composition Na (measured)
Li1*	1	1.08	1	0.69	10	10.31
Li4*	1	1.07	4	3.69	7	7.31
Li6*	1	1.04	6	6.10	5	4.90
Li8*	1	1.10	8	7.86	3	3.14
Li11*	1	1.09	11	10.45	0	0.55
LiLTA	0	0	12	11.96	0	0.04

*Where Ag_1-exchanged Li_xNa_{12-x}-LTA (x=1, 4, 6, 8, 11) samples are denoted as Li_x (x=1, 4, 6, 8, 11) respectively.

Table S2. The maximum of excitation and emission spectrum, FWHM of the emission spectrum and PLQY of Ag_1-exchanged Li_xNa_{12-x}-LTA (x=1-12) at 298 K.

Ag_1-exchanged samples	**Max. excitation (nm)**		**Max. emission (nm)**	**FWHM (cm^{-1})**	**PLQY (%)**	
					ex. 250-255	**ex. 270-285**
Li_0Na_{12}-LTA	252	279	615	3469±24	37	40
Li_1Na_{11}-LTA	252	276	610	3458±28	33	34
Li_2Na_{10}-LTA	250	279	595	3492±27	33	36
Li_3Na_9-LTA	250	278	594	3449±18	41	36
Li_4Na_8-LTA	250	277	593	3420±17	41	37
Li_5Na_7-LTA	250	277	593	3389±17	44	39
Li_6Na_6-LTA	250	276	592	3338±16	36	32
Li_7Na_5-LTA	250	277	588	3309±14	36	33
Li_8Na_4-LTA	252	276	578	3339±12	38	37
Li_9Na_3-LTA	250	274	563	3449±21	36	36
$Li_{10}Na_2$-LTA	250	272	540	3401±38	35	33
$Li_{11}Na_1$-LTA	250	273	530	3256±39	22	20
$Li_{12}Na_0$-LTA	250	274	515	3015±36	7	5

Table S3. The maximum of excitation and emission spectrum, FWHM of the emission spectrum and PLQY of Ag_1-exchanged Li_xNa_{12-x}-LTA (x=1-12) at 77 K.

Ag_1-exchanged samples	**Max. excitation (nm)**		**Max. emission (nm)**	**FWHM (cm^{-1})**	**PLQY (%)**	
					ex. 250-255	**ex. 270-285**
Li_0Na_{12}-LTA	258	283	412	2994±32	52	63
Li_1Na_{11}-LTA	257	282	405	2881±29	54	67
Li_2Na_{10}-LTA	255	280	400	2697±24	56	68
Li_3Na_9-LTA	255	281	398	2626±21	58	74
Li_4Na_8-LTA	255	280	396	2507±20	56	66
Li_5Na_7-LTA	256	279	395	2443±18	52	72
Li_6Na_6-LTA	254	279	393	2432±15	55	73
Li_7Na_5-LTA	254	279	392	2372±14	56	64
Li_8Na_4-LTA	254	279	389	2361±13	57	64
Li_9Na_3-LTA	253	276	385	2421±15	65	75
$Li_{10}Na_2$-LTA	250	275	376	2392±21	61	66
$Li_{11}Na_1$-LTA	250	275	372	2341±27	47	45
$Li_{12}Na_0$-LTA	250	272	368	2494±68	15	18

4. References

(1) Baekelant, W.; Aghakhani, S.; Coutino-Gonzalez, E.; Kennes, K.; D'Acapito, F.; Grandjean, D.; Van Der Auweraer, M.; Lievens, P.; Roeffaers, M. B. J.; Hofkens, J.; Steele, J. A. Shaping the Optical Properties of Silver Clusters Inside Zeolite A via Guest-Host-Guest Interactions. *J. Phys. Chem. Lett.* **2018**, *9* (18), 5344–5350. https://doi.org/10.1021/acs.jpclett.8b01890.

(2) Baekelant, W.; Aghakhani, S.; Coutino-Gonzalez, E.; Grandjean, D.; Kennes, K.; Jonckheere, D.; Fron, E.; D'Acapito, F.; Longo, A.; Lievens, P.; Roeffaers, M. B. J.; Hofkens, J. Confinement of Highly Luminescent Lead Clusters in Zeolite A. *J. Phys. Chem. C* **2018**, *122* (25), 13953–13961. https://doi.org/10.1021/acs.jpcc.8b01107.

(3) Fron, E.; Aghakhani, S.; Baekelant, W.; Grandjean, D.; Coutino-Gonzalez, E.; Van Der Auweraer, M.; Roeffaers, M. B. J.; Lievens, P.; Hofkens, J. Structural and Photophysical Characterization of Ag Clusters in LTA Zeolites. *J. Phys. Chem. C* **2019**, *123* (16), 10630–10638. https://doi.org/10.1021/acs.jpcc.9b00204.